

1  
2 **A molecularly distinct accumbal-to-lateral hypothalamic circuit**  
3 **modulates food seeking and consumption**

4  
5 Yiqiong Liu<sup>1,2,3</sup>, Zheng-dong Zhao<sup>1,2,3</sup>,  
6 Guoguang Xie<sup>1,2,3</sup>, Renchao Chen<sup>1,2,3</sup>, and Yi Zhang<sup>1,2,3,4,5\*</sup>

7  
8 <sup>1</sup>Howard Hughes Medical Institute, Boston Children's Hospital, Boston, Massachusetts 02115,  
9 USA; <sup>2</sup>Program in Cellular and Molecular Medicine, Boston Children's Hospital, Boston,  
10 Massachusetts 02115, USA; <sup>3</sup>Division of Hematology/Oncology, Department of Pediatrics,  
11 Boston Children's Hospital, Boston, Massachusetts 02115, USA; <sup>4</sup>Department of Genetics,  
12 Harvard Medical School, Boston, Massachusetts 02115, USA; <sup>5</sup>Harvard Stem Cell Institute,  
13 WAB-149G, 200 Longwood Avenue, Boston, Massachusetts 02115, USA.

14  
15  
16 \*To whom correspondence should be addressed

17 E-mail: [yzhang@genetics.med.harvard.edu](mailto:yzhang@genetics.med.harvard.edu)

18  
19  
20  
21 Running title: NAc *Serpinb2*<sup>+</sup> D1 MSN in food reward

22  
23 Keywords: Food intake, Nucleus accumbens, *Serpinb2*-expressing D1 neuron, motivation,  
24 Lateral hypothalamus, Leptin

25  
26 Manuscript information: 31 pages, 6 figures, 6 supplemental figures

27

28

## 29 **Abstract**

30 Understanding the mechanism of energy homeostasis is expected to lead to effective treatment to  
31 obesity and metabolic diseases<sup>1,2</sup>. However, energy homeostasis is a complicated process largely  
32 controlled by neuronal circuits in the hypothalamus and brainstem<sup>3-5</sup>, whereas reward and  
33 motivation of food intake are mainly controlled by the limbic regions<sup>6</sup> and cerebral cortex<sup>7,8</sup>.  
34 Although the limbic and hypothalamus connection like Nucleus Accumbens shell (NAcSh) to the  
35 lateral hypothalamus (LH) circuit has been reported to regulate feeding<sup>9,10</sup>, the neuron subtypes  
36 involved, and how do the humoral/neuronal signals coordinate to direct feeding behavior remain  
37 unknown. Here we show that the projection from dopamine receptor D1(Drd1)- and *Serpib2*-  
38 expressing subtype to leptin receptor (LepR) expressing neurons in LH modulates food seeking  
39 and consumption. We demonstrate that the *Serpib2*<sup>+</sup> neuronal activity is dynamically modulated  
40 during feeding. Conversely, chemo/optogenetics-mediated modulation of *Serpib2*<sup>+</sup> neurons  
41 bidirectionally regulate food seeking and consumption. Importantly, circuitry stimulation  
42 revealed the NAcSh<sup>Serpib2</sup>→LH<sup>LepR</sup> projection controls refeeding and overcomes leptin-mediated  
43 feeding suppression. Ablation of NAcSh<sup>Serpib2</sup> neurons could decrease body weight. Together,  
44 our study reveals a molecularly distinct accumbal-to-lateral hypothalamic neural circuit that  
45 controls internal state-dependent food consumption, which provides a promising therapeutic  
46 target for anorexia and obesity.

47

## 48 **Main**

49 The hypothalamus, with highly heterogenous neuronal composition<sup>11</sup>, plays a critical role in  
50 controlling feeding behavior<sup>12,13</sup>, where feeding related hormones, such as ghrelin and leptin,  
51 coordinately produce sensations of appetite and satiety leading to behavioral response<sup>14,15</sup>.  
52 Traditionally, people regard the arcuate nucleus (Arc) as a major location where LepR performs  
53 anorexic function by acting on leptin receptors (LepR) to suppress food intake and bodyweight  
54 gain<sup>16</sup>. In addition to the Arc, lateral hypothalamus (LH)<sup>17</sup> also highly expresses LepR to play a  
55 similar role. However, the specific neuronal subtype targeting LH<sup>LepR</sup> neurons beyond  
56 hypothalamus to regulate feeding remain to be elucidate. In recent years, several studies have  
57 analyzed the role of mediodorsal NAcSh in feeding<sup>10,18,19</sup> and revealed that activation of  
58 dopamine receptor 1 expressing medium spiny neurons (D1-MSNs)<sup>20,21</sup> projections to LH<sup>9,10</sup>  
59 stops ongoing food consumption. However, other studies showed that D1-MSNs activity was

60 enhanced during appetitive phase<sup>22</sup> as well as during consumption<sup>23</sup>. Although temporally  
61 distinct phases of feeding behavior, such as food seeking, food evaluation and consumption,  
62 could potentially account for such discrepancy, the neuronal heterogeneity of NAc<sup>24</sup> could  
63 underlie the seemingly conflict feeding behavior as the different studies might have manipulated  
64 different neuron subtypes with opposing functions. With the application of single cell RNA-seq  
65 and spatial transcriptome techniques to decipher the neuron heterogeneity of different brain  
66 regions<sup>25-29</sup>, we could focus on different neuron subtypes located in the NAcSh implicated in  
67 feeding behavior<sup>9,10,19,22,30,31</sup> to identify the neuron subtype(s) responsible for regulating feeding  
68 behavior.

69

### 70 ***Serpinb2*<sup>+</sup> neurons are activated in refeeding process**

71 Using iSpatial<sup>32</sup>, an algorithm that integrates single cell transcriptome and spatial transcriptomic  
72 information<sup>24</sup>, we analyzed NAc MSN subtypes with medial dorsal NAcSh distribution. We  
73 found that the *Tac2*, *serpinb2* and *Upb1* MSN subtypes exhibit distinct distribution patterns in  
74 medial dorsal NAcSh (Fig. 1a). Since D1-MSNs, but not D2-MSNs, provide the dominant source  
75 of accumbal inhibition to LH with rapid control over feeding via LH GABA neurons<sup>19,22</sup>, we  
76 focused our effort on the *Tac2* and *Serpinb2* D1-MSN subtypes. tSNE plots of scRNA-seq result  
77 indicated that the *Tac2*<sup>+</sup> neurons are mainly enriched in the D1-MSN subclusters 6 and 8, while  
78 *Serpinb2*<sup>+</sup> neurons are enriched in D1-MSN subcluster 2<sup>24</sup> (Fig. 1b). RNA-FISH further  
79 confirmed that both *Tac2* and *Serpinb2* subtypes belong to D1-MSN (co-express *Drd1*) and are  
80 mainly localized to medial dorsal NAcSh (Fig. 1c). Consequently, *Tac2*<sup>+</sup> and *Serpinb2*<sup>+</sup> MSN  
81 subtypes are good candidates with potential in mediating feeding behavior.

82

83 To determine whether *Tac2*<sup>+</sup> and *Serpinb2*<sup>+</sup> MSN subtypes can mediate feeding behavior, we  
84 first asked whether the activities of these neurons respond to feeding behavior by monitoring the  
85 *cFos* expression under three conditions: ad libitum access to food, after 18 hours of fast, and  
86 refeeding (Fig. 1d). By counting *cFos*<sup>+</sup> neurons that co-express *Serpinb2* or *Tac2* in the medial  
87 dorsal NAcSh under Ad libitum, fast and refeed conditions (Fig. 1e), we determined whether the  
88 *Serpinb2* and *Tac2* neurons respond to the different feeding status. We found fasting and  
89 refeeding both increased neuronal activities compared to Ad libitum as indicated by the  
90 increased *cFos*<sup>+</sup> neuron numbers (Fig. 1f). Importantly, most of the *Serpinb2*<sup>+</sup> neurons (~70%)

91 were activated by refeeding, but not fasting (Fig. 1g). In contrast, the *Tac2*<sup>+</sup> neurons do not  
92 respond to refeeding or fasting (Fig. 1h). Collectively, these data indicate that the majority of  
93 *Serpinb2*<sup>+</sup> neurons respond to refeeding process.

94

### 95 **The *Serpinb2*<sup>+</sup> neurons respond to eating behavior**

96 To facilitate studying the role of *Serpinb2*<sup>+</sup> neurons in the feeding process, we generated a  
97 *Serpinb2*-Cre mouse line (Extended Data Fig. 1a,b). We validated this mouse model by injecting  
98 a Cre-dependent AAV vector expressing light-gated cation channel channelrhodopsin (ChR2)  
99 and observed about 90% colocalization of *Serpinb2*::ChR2-eYFP signal with endogenous  
100 *Serpinb2* mRNA signal (Extended Data Fig. 1c), which is consistent with endogenous *Serpinb2*  
101 expression in the NAcSh as shown by Allen Brain Atlas. Thus, our *Serpinb2*-Cre mouse line can  
102 be used for studying *Serpinb2*<sup>+</sup> neurons.

103

104 To test whether *Serpinb2*<sup>+</sup> neurons are involved in regulating feeding, we used fiber photometry  
105 to monitor *Serpinb2*<sup>+</sup> neuronal activity during food seeking and consumption. To this end, we  
106 inserted an optic cannula into the NAcSh to record the total *Serpinb2*<sup>+</sup> neuronal activity  
107 (reflected by calcium reporter fluorescence intensity) by stereotaxic injection of a Cre-dependent  
108 AAV expressing the seventh-generation calcium reporter GCaMP7s into the NAcSh region of  
109 the *Serpinb2*-Cre mice. In parallel, we also implanted cannula to the *Drd1*-Cre mice for  
110 comparative study (Fig. 2a). Three weeks after the viral injection, we performed fluorescence  
111 recording during the feeding process. To monitor the activity dynamics of the *Serpinb2*<sup>+</sup> neurons,  
112 we designed 3-chamber food seeking and food consumption assay (Fig. 2d) and aligned calcium  
113 traces of mice with behavioral events that include habituation, food zone approaching, eating,  
114 and leaving (Fig. 2b, c). First, we recorded the Ca<sup>2+</sup> signals during the different feeding phases  
115 after the mice were fasted overnight. In habituation phase, mice were allowed to freely travel  
116 among the 3 chambers and we detected negligible response when mice approach the two empty  
117 food cups (Fig. 2d, first graph). In food approaching phase, when mice enter the food zone to  
118 interact with caged food pellets, the activity of the *Serpinb2*<sup>+</sup> neurons increased immediately  
119 when mice entered the food zone and lasted for seconds (Fig. 2d, second graph), indicating that  
120 *Serpinb2*<sup>+</sup> neurons respond to appetitive food seeking. In the eating phase, we observed a  
121 significant increase of Ca<sup>2+</sup> signals when mice start eating the food (Fig. 2d, 3<sup>rd</sup> graph), and

122 subsequently, declined to lower than baseline level after eating finished. Usually, mice turned  
123 away and left the food zone (Fig. 2d, 4<sup>th</sup> graphs).

124

125 To quantify the total *Serpinb2*<sup>+</sup> neuronal activity at different phases, we calculated the area under  
126 curve index (AUC) of the calcium signal curve for each trial. We find that the AUC is  
127 significantly higher in the food zone approaching and eating phases and lower in the post eating  
128 phases compared with that of habituation (Fig. 2d, right panel). In parallel experiments with the  
129 *Drd1*-Cre mice, we observed Ca<sup>2+</sup> signal tended to increase when approach to food zone (Fig. 2e,  
130 second graph) and reduce during consumption (Fig. 2e, 3<sup>rd</sup> graph). After eating, *Drd1*<sup>+</sup> neuronal  
131 activity increased concomitantly (Fig. 2e, 4<sup>th</sup> graphs). Similar results were also observed in ad  
132 libitum status (Extended Data Fig. 2). These results indicate that *Serpinb2*<sup>+</sup> neurons function  
133 differently from other *Drd1*<sup>+</sup> neurons especially in appetitive and consumption phases.

134

### 135 ***Serpinb2*<sup>+</sup> neurons bidirectionally regulate food intake in hungry state**

136 To determine whether *Serpinb2*<sup>+</sup> neuronal activity plays a causal role in regulating feeding  
137 behavior, we asked whether the feeding behavior can be changed by manipulating *Serpinb2*<sup>+</sup>  
138 neurons' activity. To this end, we applied chemogenetic techniques<sup>33</sup> to the *Serpinb2*-Cre mice  
139 by injecting the activating AAV encoding a modified human M3 muscarinic receptor (hM3Dq)  
140 or the inhibitory vector AAV-DIO-hM4Di-mCherry into the NAcSh region. As controls, we also  
141 performed parallel experiments using *Tac2*-Cre and *Drd1*-Cre mice (Extended Data Fig. 3a). We  
142 first confirmed the accuracy of the injection site (Extended Data Fig. 3b), then the efficiency of  
143 the activation and inhibition with *cFos* expression (Extended Data Fig. 3c).

144

145 We then tested whether activation or inhibition of the *Serpinb2*<sup>+</sup> neurons affect feeding and  
146 reward-related behaviors (Fig. 3a). Interestingly, under Ad libitum conditions, manipulation of  
147 the *Serpinb2*<sup>+</sup> neuronal activity does not affect food intake (Fig. 3b, left panel), indicating that  
148 the eating behavior under Ad libitum maybe controlled by other neurons. Next, we performed the  
149 same test using fasted mice to analyze total food consumption during refeeding (Fig. 3a-c). We  
150 found that activation of the *Serpinb2*<sup>+</sup> neurons increased food consumption, while inhibition of  
151 the *Serpinb2*<sup>+</sup> neurons decreased food consumption (Fig. 3b, right panel). However, similar  
152 manipulation on *Tac2*-Cre or *Drd1*-Cre mice did not affect food consumption (Fig. 3c). In

153 addition to the total food consumption, we also analyzed food preference indicated by the time  
154 spent in the food zone (Fig. 3c). As expected, fasted mice would significantly increase their time  
155 spent in the food zone for the control mouse group (Fig. 3d). Importantly, activation (hM3Dq) or  
156 inhibition (hM4Di) the *Serpinb2*<sup>+</sup> neurons respectively increased or decreased the time the mice  
157 spent in the food zone compared to that of the control mice (Fig. 3e). In contrast, similar  
158 manipulation of the *Tac2*-Cre or *Drd1*-Cre mice showed no such effect compared to that in the  
159 control mice (Fig. 3e). These results indicate that manipulation the *Serpinb2*<sup>+</sup> neuronal activity  
160 can regulate food seeking and intaking behavior in hungry state.

161  
162 To further determine whether the neuronal activity of the *Serpinb2*<sup>+</sup> neurons has a causal role in  
163 regulating food motivation, we next carried out food operant chamber test (Fig. 3f, g). To  
164 maintain a similar food motivation status, all mice were food restricted to reduce body weight to  
165 around 90% of their original value. After trained to operantly respond to sweetened chow pellets  
166 on fixed ratio (FR) 1, 3, 5 schedule, the animals were then tested for lever pressing upon CNO-  
167 induced chemogenetic manipulation. For the FR5 test, *Serpinb2*<sup>+</sup> neuron activation significantly  
168 increased the active lever pressing and pellet reward (Fig. 3h), while *Serpinb2*<sup>+</sup> neuron inhibition  
169 elicited the opposite effect (Fig. 3h). For the progressive ratio (PR) 5 test, *Serpinb2*<sup>+</sup> neuron  
170 activation showed a tendency of increased number of active lever pressing and significantly  
171 increased pellet reward (Fig. 3i), while *Serpinb2*<sup>+</sup> neuron inhibition decreased both the total  
172 active lever pressing and the reward (Fig. 3i). Taken together, these results demonstrate that the  
173 *Serpinb2*<sup>+</sup> neurons are involved in bidirectional control of goal-direct food seeking behavior.

174  
175 NAc shell is also known to regulate anxiety<sup>34</sup> and drug reward<sup>35,36</sup>. Thus, we asked whether  
176 *Serpinb2*<sup>+</sup> neurons also regulate these behaviors under the same chemogenetic manipulation. We  
177 found that manipulation of *Serpinb2*<sup>+</sup> neuronal activity does not affect locomotion in open field  
178 test (Extended Data Fig. 4a,b), or drug reward in cocaine conditioned place preference (CPP) test  
179 (Extended Data Fig. 4c), or anxiety in elevated plus maze (EPM) test (Extended Data Fig. 4d,e).  
180 Taken together, these results support that *Serpinb2*<sup>+</sup> neurons are specifically involved in food  
181 refeeding process, but not involved in locomotion, anxiety or drug seeking behaviors.

182

183 ***Serpinb2*<sup>+</sup> neurons mediate food consumption via LH projection**

184 Thus far, characterization of the *Serpinb2*<sup>+</sup> neurons was at the somatic level in NAcSh. Next, we  
185 attempt to understand how the *Serpinb2*<sup>+</sup> neurons regulate food taking behavior at the circuit  
186 level. Previous studies have indicated that NAcSh D1-MSNs could project to multiple brain  
187 regions, including ventral tegmental area (VTA)<sup>37</sup>, ventral pallidum (VP)<sup>38</sup>, and bed nucleus stria  
188 terminalis (BNST)<sup>39</sup>. To determine the projection site of *Serpinb2*<sup>+</sup> neurons, we performed  
189 anterograde tracing by injecting Cre-dependent AAVs expressing ChR2(H134R) into the NAcSh  
190 of the *Serpinb2*-Cre mice (Fig. 4a). Analysis of the brain slices after 3 weeks of virus injection  
191 revealed that the *Serpinb2*<sup>+</sup> neurons only project to lateral hypothalamus (LH) (Fig. 4a). To  
192 further validate this projection, we injected the widely used retrograde tracer Cholera toxin  
193 subunit B (CTB)<sup>40</sup> into the LH region (Fig. 4b), and observed colocalization of CTB with  
194 mCherry in the NAcSh after immunostaining of NAcSh from the *Serpinb2*-Cre mice (Fig. 4b, c),  
195 supporting the NAcSh to the LH projection.

196

197 To demonstrate that the NAcSh to the LH projection of the *Serpinb2*<sup>+</sup> neurons is functionally  
198 relevant to food intaking, we asked whether optogenetic manipulation of the *Serpinb2*<sup>+</sup> neuron  
199 terminals in LH can change the feeding behavior of the *Serpinb2*-Cre mice. To this end, DIO-  
200 ChR2-eYFP or DIO-NpHR-eYFP AAV viruses were injected to the NAcSh of the *Serpinb2*-Cre  
201 mice with optic cannula implanted into their LH region (Fig. 4d). After fasting the mice for  
202 overnight, we activated the *Serpinb2*<sup>+</sup> neuron terminals in the LH with blue light on-off  
203 stimulation (20 Hz, 2-ms pulses). We found that mice with the *Serpinb2*<sup>+</sup> neuron terminal  
204 stimulation significantly increased their food intake in 20 mins compared to the control mice that  
205 express eYFP (Fig. 4e, left panel). Conversely, *Serpinb2*<sup>+</sup> neuron terminal inhibition in the LH  
206 with yellow on-off stimulation (20 Hz, 2-ms pulses) decreased total food intake when compared  
207 with the control (Fig. 4e, right panel). Collectively, viral tracing and circuit manipulation  
208 demonstrate that the NAcSh to LH projecting *Serpinb2*<sup>+</sup> neurons have an important function in  
209 regulating food intaking behaviors.

210

### 211 ***Serpinb2*<sup>+</sup> neurons form a circuit with LH LepR<sup>+</sup> GABA<sup>+</sup> neurons**

212 Having demonstrated the functional importance of the NAcSh to LH projection, we next  
213 attempted to determine the neuron types in LH that receive signals from the *Serpinb2*<sup>+</sup> neurons.  
214 The LH is a highly heterogeneous brain region controlling food intake, energy expenditure, and

215 many other physiological functions<sup>41</sup>. Since neural peptides orexin/hypocretin and melanin-  
216 concentrating hormone (MCH) are associated with feeding<sup>42,43</sup>, and are mainly express in LH,  
217 we first asked whether they are the down-stream targets of the NAcSh *Serpib2*<sup>+</sup> neurons. To this  
218 end, we injected the AAV-DIO-ChR2 anterograde viruses to the NAcSh of the *Serpib2*-Cre  
219 mice and performed immunostaining of candidate neural peptides or transmitters on slices  
220 covering the LH (Fig. 5a). We found very few MCH- or orexin-expressing neurons in LH  
221 overlapped with *Serpib2*<sup>+</sup> terminals (Fig. 5b, indicated by arrow heads). Given that GABAergic  
222 neuron is the major subtype in the LH and has been reported to be involved in feeding and leptin-  
223 regulated energy homogenesis<sup>11,44,45</sup>, we next checked whether leptin receptor (LepR) positive  
224 GABAergic neurons<sup>17</sup> receive projections from NAcSh *Serpib2*<sup>+</sup> neurons by similar  
225 immunostaining. We found over 70% *Serpib2*<sup>+</sup> neuron terminals overlap with LepR<sup>+</sup> GABA<sup>+</sup>  
226 neurons (Fig. 5c). This data indicates that the NAcSh *Serpib2*<sup>+</sup> neurons mainly project to LepR<sup>+</sup>  
227 GABA<sup>+</sup> neurons in LH.

228  
229 To identify the brain regions that response to refeeding, we performed whole brain *cFos*  
230 mapping on the refeeding mice. By postmortem immunostaining, we found *cFos* expression was  
231 increased in multiple brain regions compared with that of ad libitum, like NAc, Olfactory  
232 tubercle (OT), paraventricular nucleus of the thalamus (PVT), Arc, Dorsomedial nucleus of the  
233 hypothalamus (DMH), LH and Zona incerta (ZI) (Fig. 5d, Extended Data Fig. 5). We next  
234 attempted to identify inputs for the NAcSh *Serpib2*<sup>+</sup> neurons by performing a modified rabies  
235 tracing experiment. To this end, the Cre-inducible avian sarcoma leucosis virus glycoprotein  
236 EnvA receptor (TVA) and rabies virus envelope glycoprotein (RG) were injected unilaterally to  
237 the NAcSh of *Serpib2*-Cre mice (Fig. 5e) to allow monosynaptic retrograde transportation and  
238 rabies virus infection in the starter neurons, respectively<sup>37,46,47</sup>. Two weeks later, the modified  
239 rabies virus SADDG-EGFP (EnvA) was injected unilaterally into the NAcSh and slices of the  
240 whole brain were imaged one week later. Confocal imaging results indicated that EGFP-labeled  
241 neurons can be found in anterior cingulate area (ACA), PVT, LH, and lateral preoptic area (LPO)  
242 (Fig. 5f, Extended Data Fig. 6), indicating that neurons in these regions send monosynaptic  
243 projection to NAcSh to form a network regulating food consumption (Fig. 5g).

244



245 Combining the major efferent regions with *cFos* mapping (Fig. 5d, f), PVT may serve as a major  
246 input for *Serpib2*<sup>+</sup> neurons in NAcSh to regulate food seeking and taking. Collectively, our  
247 study uncovered a neuronal network where the NAcSh *Serpib2*<sup>+</sup> neurons may receive signals  
248 from PVT neurons to inhibit the LepR<sup>+</sup>GABA<sup>+</sup> neurons in LH, to regulate food seeking and  
249 eating behaviors.

250

### 251 **Modulating *Serpib2*<sup>+</sup> neuronal activity can overcome leptin effect and alter bodyweight**

252 As an adipose-derived hormone, leptin plays a central role in regulating energy homeostasis<sup>48-50</sup>.  
253 Leptin performs most of its functions, including suppression of food intaking, by activating the  
254 LepR on central nerve system (CNS) neurons<sup>51,52</sup>. Since the NAcSh *Serpib2*<sup>+</sup> neurons are  
255 projected to LepR<sup>+</sup> GABAergic neurons in LH (Fig. 5c), we anticipate that both leptin and the  
256 NAcSh *Serpib2*<sup>+</sup> neurons have shared neuron targets and consequently they should have  
257 functional interaction. To analyze their functional interaction in food intaking, we implanted  
258 catheter in the LH for leptin delivery (catheter administration) on the *Serpib2*-Cre mice that  
259 were also injected with hM3Dq-mCherry-expressing AAV into the NAcSh so that the NAcSh  
260 *Serpib2*<sup>+</sup> neurons can be activated by CNO by i.p. injection. First, we established that 1 μg of  
261 bilateral intra-LH leptin cannula delivery<sup>53</sup> significantly decreased food intake in 3 hours  
262 compared to the control with saline treatment (Fig. 6a). Then we used 1 μg of leptin for all the  
263 following tests. As we have shown previously (Fig. 3b), CNO-induced *Serpib2*<sup>+</sup> neuron  
264 activation increased food intake (Fig. 6b). Importantly, although leptin delivery reduced the food  
265 intake, the leptin effect can be at least partly overcome by CNO-induced *Serpib2*<sup>+</sup> neuron  
266 activation (Fig. 6b). This data indicates that *Serpib2*<sup>+</sup> neurons' innervation to LH can at least  
267 partly overcome leptin's inhibitory effect on food intake.

268

269 To access whether loss function of the *Serpib2*<sup>+</sup> neurons can exert a long-term effect on energy  
270 homeostasis, we selectively ablated NAcSh *Serpib2*<sup>+</sup> neurons in *Serpib2*-Cre mice by injecting  
271 a flex-taCasp3-TEVp AAV expressing caspase-3 which eliminates the neurons by inducing cell  
272 death (Fig. 6c). NAcSh *Serpib2*<sup>+</sup> neurons ablation decreased food intake (Fig. 6d) as well as  
273 reduced body weight gain by 10% in 7 weeks (Fig. 6e). Together, these results demonstrate that  
274 transient change in *Serpib2*<sup>+</sup> neuronal activity could alter food seeking and consumption

275 behaviors. Modulating *Serpinb2*<sup>+</sup> neuronal activity could partly overcome leptin effect to  
276 maintain energy homeostasis, and ablation of *Serpinb2*<sup>+</sup> neurons can lead to bodyweight loss.

277

278

## 279 Discussion

280 Feeding is an essential goal-directed behavior that is heavily influenced by homeostatic state and  
281 motivation. The accumbal-to-lateral hypothalamic pathway has been implicated in regulating  
282 feeding behavior, but the specific neuron subtypes and precise neuronal circuit in LH are not  
283 clear. In this study, we filled in this knowledge gap by delineating a circuit which integrates  
284 neuronal and humoral signal to regulate food consumption in an innate energy state-dependent  
285 manner. Specifically, we identified a D1-MSN subtype located in the NAcSh and expresses  
286 *Serpinb2* to regulate the feeding behavior through a neuronal circuit involving  
287 NAcSh<sup>*Serpinb2*</sup>→LH<sup>LepR</sup> that is beyond the hypothalamus. We demonstrate that the *Serpinb2*<sup>+</sup>  
288 neurons bidirectionally modulate food motivation and consumption specifically in hungry state.  
289 Importantly, *Serpinb2*<sup>+</sup> neurons target the LepR expressing GABAergic neurons in LH and their  
290 activation can at least partly overcome the suppressive effect of leptin on food intaking, and  
291 whose ablation can chronically cause bodyweight loss.

292

### 293 The *Serpinb2*<sup>+</sup> neurons are functionally distinct from the pan D1-MSNs in NAcSh

294 Previous studies have observed reduced D1 firing during food consumption, and consistently,  
295 suppressing D1-MSNs activity prolonged food intake<sup>19</sup>. Using *Serpinb2*-Cre and *Drd1*-Cre mice,  
296 we compared the *Serpinb2*<sup>+</sup> MSNs neurons and the D1-MSNs in regulating feeding behaviors  
297 (Fig. 2, 3), and found their manipulation have different outcomes. First, *Serpinb2*<sup>+</sup> neurons are  
298 activated by both food approaching and food consumption, while *D1*<sup>+</sup> neurons show bi-phasic  
299 response, activated during food approaching but suppressed during food consumption. Second,  
300 *Serpinb2*<sup>+</sup> neurons bidirectionally regulate food seeking and intake, particularly during refeeding,  
301 while *D1*<sup>+</sup> neuron manipulation does not significantly alter feeding behavior. On the other hand,  
302 a previous study showed that *D1*<sup>+</sup> neuron inhibition promoted liquid fat food intake<sup>19</sup>. This  
303 difference might be due to the different feeding assays used in the two studies, while we used  
304 free-access chow food intake, the previous study used a head-fixed mice licking liquid fat food  
305 as the assay<sup>19</sup>. Third, *Serpinb2*<sup>+</sup> neuron ablation significantly reduced food intake (Fig. 6), which

306 is consistent with our finding that *SerpinB2*<sup>+</sup> neuron activation positively regulates food intake  
307 (Fig. 3). However, a previous study indicated that lesions or inactivation of the NAc neurons do  
308 not significantly alter the food consumption<sup>54</sup>. We do not consider these results to be in conflict  
309 as NAc is composed of many D1- and D2-MSN neuron subtypes, of which many are not  
310 involved in regulating food intake, while others can positively or negatively regulate food intake.  
311 Consequently, manipulating *Serpinb2*<sup>+</sup> neurons and the entire NAc neurons can have totally  
312 different outcomes. This further indicates that finer granularity and cell type-specific approaches  
313 are needed to dissect the function of different neuron subtypes in NAc. For example, although  
314 the *D2*<sup>+</sup> neuronal activity as a whole is not altered during food consumption<sup>19,22</sup>, the D2 receptors  
315 are indeed downregulated in obese rodent as well as human<sup>55,56</sup>, whether certain D2-MSN  
316 subtypes are involved in regulating food intake remains to be determined.

317

### 318 ***Serpinb2*<sup>+</sup> and *Tac2*<sup>+</sup> MSNs respectively modulate food and drug reward**

319 The NAcSh has long been implicated in regulating reward-related behaviors that are associated  
320 with food, social, and drug. Previous studies were mainly based on dichotomous MSNs subtypes  
321 that express dopamine receptor 1 or dopamine receptor 2 (D1- or D2-MSNs)<sup>57</sup>. Increasing  
322 evidence suggest that the NAcSh is highly heterogeneous in terms of the molecular features and  
323 anatomical connections of the neurons located in this region. This raises an interesting question  
324 that whether these reward-related behaviors are regulated by distinct or overlap neuron subtypes  
325 and/or projections. By combining iSpatial analysis, *cFos* mapping, neuronal activity  
326 manipulation of different subtypes, and behavioral tests, we found that the *Serpinb2*<sup>+</sup> D1-MSNs  
327 of NAcSh specifically regulate food reward, but not drug reward or other emotional and  
328 cognitive functions (Fig. 1, 3, Extended Data Fig. 4). On the other hand, we have previously  
329 showed that the *Tac2*<sup>+</sup> D1-MSNs of NAcSh specifically regulate cocaine reward<sup>58</sup>. These studies  
330 indicate that different reward behaviors are at least partly regulated by distinct MSNs subtypes.  
331 An important task for future studies will be to identify the relevant neuron subtypes regulating  
332 the various reward-related behaviors, and eventually to link the cellular heterogeneity to  
333 functional diversity of each brain regions. This way, the cellular and circuit mechanisms  
334 underlying the various behaviors can be elucidated.

335

### 336 **The PVT- NAcSh *Serpinb2*<sup>+</sup> -LH *LepR*<sup>+</sup> circuit controls feeding in hungry state**

337 Previous studies have shown that either LH GABA or Vglut2 neuronal subpopulation can  
338 receive NAc innervation<sup>19,59</sup>. However, the LH GABA and Vglut2 neurons are extremely  
339 heterogeneous, and can be further divided into 15 distinct populations, respectively<sup>60</sup>. Thus, the  
340 specific cell types that receive NAc innervation were unknown. Previous studies also showed  
341 that NAcSh D1- MSN to LH inhibitory transmission stops eating, and endocannabinoids  
342 mediated suppression of this projection promotes excessive eating of highly palatable chow<sup>61</sup>,  
343 but the D1 subtype involved in this projection was not known. Using viral tracing, we discovered  
344 that the NAcSh *Serpib2*<sup>+</sup> D1-MSNs project to *LepR*<sup>+</sup> neurons in LH underlying the *Serpib2*<sup>+</sup>  
345 neuron function in food intake (Fig. 6c). Distributed in numerous regions involved in the  
346 regulation of energy balance, the *LepR*<sup>+</sup> neurons lie in the mediobasal hypothalamic (MBH)  
347 “satiety centers” and in LH that is regarded as the “feeding center”<sup>50,62</sup>. Leptin treatment induced  
348 *cFos* expression and 100 nM of leptin depolarized 34% of *LepR*-expressing neurons in LH<sup>17</sup>.  
349 Unilateral intra-LH leptin decreased food intake and bodyweight<sup>17</sup>. In our study, we found  
350 activation of the *Serpib2*<sup>+</sup> neurons increased the inhibition of the *LepR*<sup>+</sup> neurons excitability,  
351 resulting in increased food consumption; while inhibition of *Serpib2*<sup>+</sup> neurons decreased the  
352 inhibition of *LepR*<sup>+</sup> neurons excitability, leading to decreased food consumption even after  
353 fasting (Fig. 3b, 4e). Our results are consistent with previous reports demonstrating that LH  
354 *LepR* neuron activation decreased chow intake<sup>63</sup>. Importantly, manipulating *Serpib2*<sup>+</sup> neuronal  
355 activity could override leptin’s effect in LH to modulate food consumption (Fig. 6b). It is not  
356 clear whether the lack of effect of the *Serpib2*<sup>+</sup> neurons on feeding behavior in ad libitum is due  
357 to the lack of food taking motivation or the relatively high leptin level masked the *Serpib2*<sup>+</sup>  
358 neuron effect. Alternatively, it is possible that the endocannabinoid and leptin signaling may  
359 interact in LH, where activation of NAcSh *Serpib2*<sup>+</sup> neurons suppresses *LepR* neurons in the  
360 LH, which may increase the synthesis and release of endocannabinoids<sup>64</sup> and thus promote  
361 feeding. Our study thus reveals a parallel and compensatory circuit from NAcSh to LH<sup>LepR</sup>,  
362 which is beyond the hypothalamus circuit that directly modulates food intake, to maintain energy  
363 homeostasis.

364

365 For the efferent site, *Serpib2*<sup>+</sup> neurons majorly receive input from PVT based on the GFP<sup>+</sup> cell  
366 numbers (Fig. 5f), which is believed to be an integration hub processing information and sending  
367 “command” to the downstream targets<sup>65-67</sup>. Previous studies revealed that the *Slc2a2*<sup>+</sup> neurons in

368 PVT are activated by hypoglycemia and their activation by optogenetics increases motivated  
369 sucrose seeking behavior<sup>68</sup>. On the other hand, the *Gck*<sup>+</sup> neurons in PVT have the opposite  
370 glucose sensing property as their optogenetic activation decreased sucrose seeking behavior<sup>69</sup>.  
371 Taken together, we believe that in hungry state, PVT receives the “hungry signal” and send it to  
372 *Serpinb2*<sup>+</sup> neurons. The activated *Serpinb2*<sup>+</sup> neurons then instruct the LH *LepR*<sup>+</sup> neurons to  
373 promote eating. This PVT- NAcSh *Serpinb2*<sup>+</sup> -LH *LepR*<sup>+</sup> circuit controls feeding in hungry stage and  
374 strengthens the sentinel role of NAcSh<sup>19,70</sup>.

375

### 376 ***Serpinb2*<sup>+</sup> neurons connect energy homeostasis and motivation**

377 Feeding is an essential goal-directed behavior that is influenced by cellular homeostasis state and  
378 appetitive motivation. Interestingly, we found that *Serpinb2*<sup>+</sup> neurons promote feeding in hunger  
379 state, rather than in normal feeding state, suggesting that *Serpinb2*<sup>+</sup> neuron function is regulated  
380 in an internal metabolic state-dependent manner. Consistently, ablation of *Serpinb2*<sup>+</sup> neurons  
381 significantly reduced food intake and leading to bodyweight loss (Fig. 6e,f). The *Serpinb2*<sup>+</sup>  
382 neurons are activated by both appetitive food approaching and food consumption. To measure  
383 appetitive food motivation, we conducted operant food intake assay, where mice need to press  
384 levers to earn food pellets. We found that *Serpinb2*<sup>+</sup> neuronal activity bi-directionally regulates  
385 active lever presses and the earned reward (Fig. 3h,i). These studies suggested that *Serpinb2*<sup>+</sup>  
386 neurons regulate both energy homeostasis and appetitive motivation which is consistent with the  
387 demonstrated function of NAc in integrating descending signals pertaining to homeostatic needs  
388 and goal-related behaviors<sup>3,71</sup>. Collectively, these data indicate that lose function of the NAcSh  
389 *Serpinb2*<sup>+</sup> neurons can disrupt energy homeostasis and appetitive motivation, which provides a  
390 potential therapeutic target for obese treatment. Conversely, activation of the NAcSh *Serpinb2*<sup>+</sup>  
391 neurons can be a potential strategy for anorexia treatment.

392

393 In conclusion, we identified a molecularly defined neuron population with crucial functions in  
394 regulating food intake via neuron-hormone axis. From a therapeutic point of view, our findings  
395 are highly relevant because activating or ablating a small population of molecularly defined  
396 neurons could respectively rescue food intake at low energy status or lead to long-term  
397 bodyweight loss. Given its function, we believe the small population of NAcSh *Serpinb2*<sup>+</sup>

398 neurons is an ideal entry point for understanding the complex brain-metabolism regulatory  
399 network underlying eating and bodyweight control.

400

401

402

403 **Methods**

---

404  
405 **Mice**

406 All experiments were conducted in accordance with the National Institute of Health Guide for  
407 Care and Use of Laboratory Animals and approved by the Institutional Animal Care and Use  
408 Committee (IACUC) of Boston Children's Hospital and Harvard Medical School. The *Serp1b2*-  
409 Cre mice were generated as described below. For behavioral assays, 12 -16 weeks old male mice  
410 were used. The mice were housed in groups (3-5 mice/cage) in a 12-hr light/dark cycle, with  
411 food and water ad libitum unless otherwise specified. The Tac2-Cre knock-in mouse line was a  
412 gift from Q. Ma at Dana-Farber Cancer Institute and Harvard Medical School. The D1-cre mouse  
413 line was obtained from Jackson Laboratory (JAX: 037156).

414  
415 **Fluorescence *in situ* hybridization (FISH) and immunofluorescence (IF) staining**

416 Mice were transcardially perfused with PBS followed by 4% paraformaldehyde. Brains were  
417 then placed in a 30% sucrose solution for 2 days. The brains were frozen in Optimal Cutting  
418 Temperature (OCT) embedding media and 16  $\mu$ m (for FISH) or 40  $\mu$ m (for IF) coronal sections  
419 were cut with vibratome (Leica, no. CM3050 S). For FISH experiments, the slices were mounted  
420 on SuperFrost Plus slides, and air dried. The multi-color FISH experiments were performed  
421 following the instructions of RNAscope Fluorescent Multiplex Assay (ACD Bioscience). For IF,  
422 cryostat sections were collected and incubated overnight with blocking solution (1 $\times$ PBS  
423 containing 5% goat serum, 5% BSA, and 0.1% Triton X-100), and then incubated with the  
424 following primary antibodies, diluted with blocking solution, for 1 day at 4  $^{\circ}$ C. Samples were  
425 then washed three times with washing buffer (1 $\times$ PBS containing 0.1% Tween-20) and incubated  
426 with the Alexa Fluor conjugated secondary antibodies for 2 h at room temperature. The sections  
427 were mounted and imaged using a Zeiss LSM800 confocal microscope or an Olympus VS120  
428 Slide Scanning System. Antibodies used for staining were as follows: rabbit anti-cFos (1:2000,  
429 Synaptic systems, #226003), chicken anti-GFP (1:2000, Aves Labs, no. GFP-1010), chicken  
430 anti-mCherry (1:2000, Novus Biologicals, no. NBP2-25158), Orexin-A (KK09) antibody, (1:500,  
431 Santa Cruz Biotechnology, Cat# sc-80263 ), anti-MCH, Ab1-pmch antibody (1:2000, Phoenix  
432 Pharmaceuticals, Cat# H-070-47 ), Anti-GABA antibody (1:1000, Sigma, Cat# A2052) , Leptin  
433 Receptor antibody (Abcam, Cat# ab104403), Goat anti-chicken Alexa Fluor 488(Thermo Fisher

434 Scientific, Cat# A11039), Donkey anti-rabbit Alexa Fluor 488(Thermo Fisher Scientific, Cat#  
435 A21206), Donkey anti-rabbit Alexa Fluor 568(Thermo Fisher Scientific, Cat# A10042).

436

#### 437 **AAV vectors**

438 The following AAV vectors (with a titer of  $>10^{12}$ ) were purchased from UNC Vector Core:  
439 AAV5-EF1a-DIO-hChR2(H134R)-EYFP, AAV5-EF1a-DIO-EYFP, AAV-DJ-  
440 EF1a-DIO-GCaMP6m. The following AAV vectors were purchased from Addgene: AAV5-  
441 hSyn-DIO-hM3D(Gq)-mCherry (#44361), AAV5-hSyn-DIO-hM4D(Gi)-mCherry (#44362),  
442 AAV5-hSyn-DIO-mCherry (#50459), pAAV-flex-taCasp3-TEVp (#45580), pAAV-Ef1 $\alpha$ -DIO  
443 eNpHR 3.0-EYFP (#26966), EnvA G-deleted Rabies-EGFP (Salk Institute).

444

#### 445 **Stereotaxic brain surgeries**

446 The AAV vectors were injected through a pulled-glass pipette and the nanoliter injector  
447 (Nanoject III, Drummond Scientific - 3-000-207). The injection was performed using a small-  
448 animal stereotaxic instrument (David Kopf Instruments, model 940) under general anesthesia by  
449 isoflurane (0.8 liter/min, isoflurane concentration 1.5%) in oxygen. A feedback heater was used  
450 to keep mice warm during surgeries. Mice were allowed to recover in a warm blanket before  
451 they were transferred to housing cages for 2–4 weeks before behavioral evaluation was  
452 performed. For chemogenetics experiments, 0.1~0.15  $\mu$ l of AAV vector was bilaterally delivered  
453 into target regions. For optogenetics experiments, following viral injection, the fiber optic  
454 cannula (200  $\mu$ m in diameter, Inper Inc.) were implanted 0.1 mm above viral injection site and  
455 were secured with dental cement (Parkell, #S380). For the drug delivery cannula implantation,  
456 the cannula (Guide cannula: C.C 2.0mm, C=4.5mm; Injector: G1=0.5mm; Dummy cannula:  
457 G2=0, RWD Life Science) were directly implanted 0.5 mm above the LH and were secured with  
458 dental cement (Parkell, #S380). The coordinates of viral injection sites are based on previous  
459 literature as follow: NAc (anterior-posterior [AP] +1.2, medial-lateral [ML]  $\pm$  0.6, dorsal-ventral  
460 [DV] -4.5 mm) and LH (AP -1.3, ML  $\pm$  1.2, DV -5.0 mm).

461

#### 462 **Neuronal Tracing**

463 For CTB tracing, mice were injected with 100–200  $\mu$ l CTB-647 (AF-CTB, all from Life  
464 Technologies) unilaterally into the LH (AP -1.2, ML +1.2, DV -4.75 mm). For rabies tracing,



465 *Serpinb2-cre* mice were first unilaterally injected in the NAcSh with the starter AAV. After 14 d,  
466 the same mice were injected with the rabies virus. Then, 11 days after CTB injections and 7 days  
467 after rabies injections, brains tissue was collected and processed for confocal imaging. To aid  
468 visualization, images were adjusted for brightness and contrast using ImageJ, but alterations  
469 always were applied to the entire image.

470

## 471 **Behavioral assays**

472

473 **Open-field tests (OFT).** A clear box (square 27.3 cm x 27.3 cm square base with 20.3 cm high  
474 walls) used for the open field test, and the center zone was 50% of the total area. Prior to testing,  
475 mice were habituated to the test room for at least 20 minutes. Mice were placed in the center of  
476 the box at the start of the assay. Movement was recorded using a measurement (Med Associates,  
477 St. Albans, VT, ENV-510) 1 hour in 5 mins bins. In addition to regular parameters related to  
478 locomotor activity (such as total travel distance, velocity, ambulatory time, resting time), time  
479 spent, and distance travelled in the center area of the testing arena were also recorded and  
480 analyzed.

481

482 **Elevated plus maze (EPM).** EPM was used to measure anxiety effect. Before EPM test, mice  
483 were brought to the testing room for environmental habituation for at least 30 min. The EPM  
484 apparatus is consisted of an elevated platform (80 cm above the floor), with four arms (each arm  
485 is 30 cm in length and 5 cm in width), two opposing closed arms with 14 cm walls and two  
486 opposing open arms. Mice were attached into the fiber-optic patch cord and were individually  
487 placed in the center of the EPM apparatus, towards one of the open arms. The mice trajectories  
488 were tracked for 5 minutes, and the time spent in the open arms was analyzed using Ethovision  
489 XT11 (Noldus).

490

491 **Cocaine conditioned place preference (cocaine-CPP).** Mice were allowed to freely explore  
492 both sides of a custom-made (Med Associates) CPP training apparatus (25 × 19 × 17 cm for L ×  
493 D × H) for 30 min. Trajectories were tracked by infra-red photobeam detectors, and the travel  
494 distance and the duration were recorded to assess their baseline place preference. Mice that  
495 showed strong bias (< 25% preference) were excluded from the experiments. Then, for

496 chemogenetic activation or inhibition during CPP formation, these mice were injected with  
497 saline (i.p.) and confined to their preferred side of the chamber for 30 min before returned to  
498 their home cage. At least four hours later, the same mice received CNO at least 15 min before an  
499 i.p. injection of 15 mg/Kg cocaine and were confined to their non-preferred side of the chamber  
500 for 30 minutes. They were then returned to their home cage. The same training with saline and  
501 CNO injection were performed for three consecutive days. Twenty-four hours after the final  
502 training session, mice were re-exposed to the CPP chamber and allowed to explore both sides of  
503 the chamber for 30 min.

504

505 **Post-fasted food intake.** Mice were individually placed in the home cage and fasted overnight  
506 (18 hours). Mice received N-clozapine (CNO, 2mg/mL for hM3Dq group and 5mg/mL for  
507 hM4Di group) via i.p. injection and then regular chow pellets (3 g per pellet) were put in the  
508 hopper. Three hours later, the remaining food pellets were collected and measured to calculate  
509 total amount of food consumed (g). For the leptin treatment test, 15 mins after CNO injection, 1  
510  $\mu$ g of leptin (R&D, Cat# 498-OB) was delivered through cannula by pump for 5 mins and waited  
511 for another 5 mins before adding pellets. For the Ta-Casp3 treatment group, the test was carried  
512 out 3 weeks after virus injection.

513

514 **Food place preference.** Animals were placed in a custom three-chamber, 45  $\times$  60  $\times$  35 cm arena  
515 to assess the amount of food consumed and time spent in a designated food zone area. The arena  
516 contained two 64-cm<sup>2</sup> food cups in two outer corners of separate chambers. One cup contained  
517 standard grain-based chow (Harlan, Indianapolis, IN), while the other cup remained empty. Mice  
518 were allowed to explore the arena freely, and spatial locations were tracked using EthoVision XT  
519 10 (Noldus, Leesburg, VA) and CCD cameras (SuperCircuits, Austin, TX).

520

521 **Operant behavior.** Animals were first given access to 20 mg sweetened chow pellets in their  
522 home cage before testing. Animals were then trained to enter the chamber to retrieve a pellet.  
523 Each pellet was delivered 10 s after the prior pellet retrieval. After at least 2 days training and  
524 until >30 pellets earned in a single session, animals were trained for the fixed ration 1 (FR1) task,  
525 in which each active lever pressing was rewarded with a pellet. A new trial does not begin until  
526 animals entered the magazine to retrieve the pellet. Retrieval was followed by a 5 s intertrial

527 interval, after which the levers were reactivated, indicated by a cue light. Training continued  
528 until >40 pellets were earned in a single 60 mins session.

529

530 **Progressive ratio.** After FR1, FR3, FR5 training sessions, all mice were tested with CNO  
531 treatment. For progressive ratio (PR) task, a schedule of reinforcement, each subsequent reward  
532 required exponentially more lever pressing based on the formula  $(5 \times e^{0.2n}) - 5$ , rounded to the  
533 nearest integer, where  $n$  = number of rewards earned<sup>72</sup>. 60 mins per session.

534

### 535 **Optogenetic modulations of post-fasted food intake**

536 Mice received 20 min laser stimulation (4 × 5 min, On-Off-On-Off), and then the remaining food  
537 pallets were collected and food intake was measured. For photostimulating ChR2, a 473-nm laser  
538 (OEM Lasers/OptoEngine) was used to generate laser pulses (10-15 mW at the tip of the fiber, 5  
539 ms, 20 Hz) throughout the behavioral session, except when noted otherwise, controlled by a  
540 waveform generator (Keysight). For NpHR photostimulation, a 532-nm laser (OEM  
541 Lasers/OptoEngine) generated constant light of 8-10 mW power at each fiber tip.

542

### 543 **Fiber photometry during feeding**

544 The *Serpib2*<sup>+</sup> neuronal dynamics during feeding was measured using fiber photometry.  
545 Following injection of an AAV1-hSyn-FLEX-GCaMP7s vector into NAcSh of *Serpib2*-Cre  
546 mice, an optical cannula (Ø200 µm core, 0.37 numerical aperture) was implanted 100 µm above  
547 the viral injection site. Mice were allowed to recover for 3 weeks and then subjected to  
548 behavioral test. GCaMP fluorochrome was excited, and emission fluorescence was acquired with  
549 the RZ10X fiber photometry system, which has built-in LED drivers, LEDs, and photosensors  
550 (Tucker-Davis Technologies). The LEDs include 405 nm (as isosbestic control) and 465 nm (for  
551 GCaMP excitation). Emitted light was received through the Mini Cube (Doric Lenses) and split  
552 into two bands, 420 to 450 nm (autofluorescence) and 500 to 550 nm (GCaMP7 signal). Mice  
553 with optical cannula were attached to recording optic cables, and the LED power at the tip of the  
554 optical cables was adjusted to the lowest possible (~20 µW) to minimize bleaching. Mice were  
555 placed in the 3- chamber for food preference and food consumption test. Mice behaviors were  
556 recorded using EthoVision XT 10 (Noldus, Leesburg, VA) and CCD cameras (Super Circuits,  
557 Austin, TX).

558

559 For the 3-chamber food seeking and food consumption, mice were fasted overnight, and were  
560 then habituated for 10-min in the chamber that contain 2 empty food cups, after that, we put a  
561 non-eatable object and food pellets in the two food cups, during this phase, food pellets are caged  
562 so that mice can sense the food but are unable to eat them. After 10-min recording, we then  
563 removed the barrier of food and mice have free-access to the food, mice eating events were then  
564 recorded. Behavioral events, such as baseline of free moving, entering food zone, food  
565 consumption and post eating were scored manually and synchronized with fluorescence signal  
566 based on recorded videos. The voltage signal data stream was acquired with Synapse software  
567 (Tucker-Davis Technologies) and were exported, filtered, and analyzed with custom-written  
568 Matlab code. To calculate  $\Delta F/F$ , a polynomial linear fitting was applied to isosbestic signal to  
569 align it to the GCaMP7 signal, producing a fitted isosbestic signal that was used to normalize the  
570 GCaMP7 as follows:  $\Delta F/F = (\text{GCaMP7signal} - \text{fitted isosbestic})/\text{fitted isosbestic signal}$ .

571

#### 572 **Lead Contact**

573 Further information and requests for reagents should be directed to and will be fulfilled by the  
574 Lead Contact, Yi Zhang ([yzhang@genetics.med.harvard.edu](mailto:yzhang@genetics.med.harvard.edu)).

575

#### 576 **Data and Code Availability**

577 The custom code that supports the findings from this study are available from the Lead Contact  
578 upon request.

579

580

581 **Reference**

582

- 583 1 Giel, K. E. *et al.* Binge eating disorder. *Nat Rev Dis Primers* **8**, 16, doi:10.1038/s41572-022-  
584 00344-y (2022).
- 585 2 Kaye, W. H., Fudge, J. L. & Paulus, M. New insights into symptoms and neurocircuit function of  
586 anorexia nervosa. *Nature Reviews Neuroscience* **10**, 573-584, doi:10.1038/nrn2682 (2009).
- 587 3 Rossi, M. A. & Stuber, G. D. Overlapping Brain Circuits for Homeostatic and Hedonic Feeding.  
588 *Cell Metab* **27**, 42-56, doi:10.1016/j.cmet.2017.09.021 (2018).
- 589 4 Zhan, C. *et al.* Acute and long-term suppression of feeding behavior by POMC neurons in the  
590 brainstem and hypothalamus, respectively. *The Journal of neuroscience : the official journal of*  
591 *the Society for Neuroscience* **33**, 3624-3632, doi:10.1523/JNEUROSCI.2742-12.2013 (2013).
- 592 5 Li, Y. *et al.* Serotonin neurons in the dorsal raphe nucleus encode reward signals. *Nat Commun* **7**,  
593 10503, doi:10.1038/ncomms10503 (2016).
- 594 6 Dietrich, M. O. *et al.* AgRP neurons regulate development of dopamine neuronal plasticity and  
595 nonfood-associated behaviors. *Nature neuroscience* **15**, 1108-1110, doi:10.1038/nn.3147 (2012).
- 596 7 Kolb, B. & Nonneman, A. J. Prefrontal cortex and the regulation of food intake in the rat. *J Comp*  
597 *Physiol Psychol* **88**, 806-815, doi:10.1037/h0076397 (1975).
- 598 8 Davidson, T. L. *et al.* Contributions of the hippocampus and medial prefrontal cortex to energy  
599 and body weight regulation. *Hippocampus* **19**, 235-252, doi:10.1002/hipo.20499 (2009).
- 600 9 Pecina, S. & Berridge, K. C. Hedonic hot spot in nucleus accumbens shell: where do mu-opioids  
601 cause increased hedonic impact of sweetness? *The Journal of neuroscience : the official journal*  
602 *of the Society for Neuroscience* **25**, 11777-11786, doi:10.1523/JNEUROSCI.2329-05.2005  
603 (2005).
- 604 10 Thoeni, S., Loureiro, M., O'Connor, E. C. & Luscher, C. Depression of Accumbal to Lateral  
605 Hypothalamic Synapses Gates Overeating. *Neuron* **107**, 158-172 e154,  
606 doi:10.1016/j.neuron.2020.03.029 (2020).
- 607 11 Chen, R., Wu, X., Jiang, L. & Zhang, Y. Single-Cell RNA-Seq Reveals Hypothalamic Cell  
608 Diversity. *Cell reports* **18**, 3227-3241, doi:10.1016/j.celrep.2017.03.004 (2017).
- 609 12 Li, Y. *et al.* Hypothalamic Circuits for Predation and Evasion. *Neuron* **97**, 911-924 e915,  
610 doi:10.1016/j.neuron.2018.01.005 (2018).
- 611 13 Waterson, M. J. & Horvath, T. L. Neuronal Regulation of Energy Homeostasis: Beyond the  
612 Hypothalamus and Feeding. *Cell Metab* **22**, 962-970, doi:10.1016/j.cmet.2015.09.026 (2015).
- 613 14 Wren, A. M. *et al.* Ghrelin enhances appetite and increases food intake in humans. *J Clin*  
614 *Endocrinol Metab* **86**, 5992, doi:10.1210/jcem.86.12.8111 (2001).
- 615 15 Myers, M. G., Cowley, M. A. & Munzberg, H. Mechanisms of leptin action and leptin resistance.  
616 *Annual review of physiology* **70**, 537-556, doi:10.1146/annurev.physiol.70.113006.100707 (2008).
- 617 16 Cowley, M. A. *et al.* Leptin activates anorexigenic POMC neurons through a neural network in  
618 the arcuate nucleus. *Nature* **411**, 480-484, doi:10.1038/35078085 (2001).
- 619 17 Leininger, G. M. *et al.* Leptin acts via leptin receptor-expressing lateral hypothalamic neurons to  
620 modulate the mesolimbic dopamine system and suppress feeding. *Cell Metab* **10**, 89-98,  
621 doi:10.1016/j.cmet.2009.06.011 (2009).
- 622 18 Loureiro, M. *et al.* Social transmission of food safety depends on synaptic plasticity in the  
623 prefrontal cortex. *Science* **364**, 991-995, doi:10.1126/science.aaw5842 (2019).
- 624 19 O'Connor, E. C. *et al.* Accumbal D1R Neurons Projecting to Lateral Hypothalamus Authorize  
625 Feeding. *Neuron* **88**, 553-564, doi:10.1016/j.neuron.2015.09.038 (2015).
- 626 20 Kreitzer, A. C. & Malenka, R. C. Striatal plasticity and basal ganglia circuit function. *Neuron* **60**,  
627 543-554, doi:10.1016/j.neuron.2008.11.005 (2008).
- 628 21 Gerfen, C. R. & Surmeier, D. J. Modulation of striatal projection systems by dopamine. *Annual*  
629 *review of neuroscience* **34**, 441-466, doi:10.1146/annurev-neuro-061010-113641 (2011).

- 630 22 Matikainen-Ankney, B. A. *et al.* Enhanced food motivation in obese mice is controlled by D1R  
631 expressing spiny projection neurons in the nucleus accumbens. *bioRxiv*, 2022.2001.2012.476057,  
632 doi:10.1101/2022.01.12.476057 (2022).
- 633 23 Tan, B. *et al.* Dynamic processing of hunger and thirst by common mesolimbic neural ensembles.  
634 *Proceedings of the National Academy of Sciences of the United States of America* **119**,  
635 e2211688119, doi:10.1073/pnas.2211688119 (2022).
- 636 24 Chen, R. *et al.* Decoding molecular and cellular heterogeneity of mouse nucleus accumbens.  
637 *Nature neuroscience* **24**, 1757-1771, doi:10.1038/s41593-021-00938-x (2021).
- 638 25 Sylwestrak, E. L. *et al.* Cell-type-specific population dynamics of diverse reward computations.  
639 *Cell* **185**, 3568-3587 e3527, doi:10.1016/j.cell.2022.08.019 (2022).
- 640 26 Osterhout, J. A. *et al.* A preoptic neuronal population controls fever and appetite during sickness.  
641 *Nature* **606**, 937-944, doi:10.1038/s41586-022-04793-z (2022).
- 642 27 Bhattacharjee, A. *et al.* Cell type-specific transcriptional programs in mouse prefrontal cortex  
643 during adolescence and addiction. *Nat Commun* **10**, 4169, doi:10.1038/s41467-019-12054-3  
644 (2019).
- 645 28 Ilanges, A. *et al.* Brainstem ADCYAP1(+) neurons control multiple aspects of sickness behaviour.  
646 *Nature* **609**, 761-771, doi:10.1038/s41586-022-05161-7 (2022).
- 647 29 Moffitt, J. R. *et al.* Molecular, spatial, and functional single-cell profiling of the hypothalamic  
648 preoptic region. *Science* **362**, doi:10.1126/science.aau5324 (2018).
- 649 30 Bond, C. W. *et al.* Medial Nucleus Accumbens Projections to the Ventral Tegmental Area  
650 Control Food Consumption. *The Journal of neuroscience : the official journal of the Society for*  
651 *Neuroscience* **40**, 4727-4738, doi:10.1523/JNEUROSCI.3054-18.2020 (2020).
- 652 31 Durst, M., Konczol, K., Balazsa, T., Eyre, M. D. & Toth, Z. E. Reward-representing D1-type  
653 neurons in the medial shell of the accumbens nucleus regulate palatable food intake. *Int J Obes*  
654 *(Lond)* **43**, 917-927, doi:10.1038/s41366-018-0133-y (2019).
- 655 32 Zhang, C., Chen, R. & Zhang, Y. Accurate inference of genome-wide spatial expression with  
656 iSpatial. *Sci Adv* **8**, eabq0990, doi:10.1126/sciadv.abq0990 (2022).
- 657 33 Alexander, G. M. *et al.* Remote control of neuronal activity in transgenic mice expressing  
658 evolved G protein-coupled receptors. *Neuron* **63**, 27-39, doi:10.1016/j.neuron.2009.06.014 (2009).
- 659 34 Kirouac, G. J. The Paraventricular Nucleus of the Thalamus as an Integrating and Relay Node in  
660 the Brain Anxiety Network. *Front Behav Neurosci* **15**, 627633, doi:10.3389/fnbeh.2021.627633  
661 (2021).
- 662 35 West, E. A. & Carelli, R. M. Nucleus Accumbens Core and Shell Differentially Encode Reward-  
663 Associated Cues after Reinforcer Devaluation. *The Journal of neuroscience : the official journal*  
664 *of the Society for Neuroscience* **36**, 1128-1139, doi:10.1523/JNEUROSCI.2976-15.2016 (2016).
- 665 36 Di Chiara, G. *et al.* Dopamine and drug addiction: the nucleus accumbens shell connection.  
666 *Neuropharmacology* **47 Suppl 1**, 227-241, doi:10.1016/j.neuropharm.2004.06.032 (2004).
- 667 37 Watabe-Uchida, M., Zhu, L., Ogawa, S. K., Vamanrao, A. & Uchida, N. Whole-brain mapping of  
668 direct inputs to midbrain dopamine neurons. *Neuron* **74**, 858-873,  
669 doi:10.1016/j.neuron.2012.03.017 (2012).
- 670 38 Pardo-Garcia, T. R. *et al.* Ventral Pallidum Is the Primary Target for Accumbens D1 Projections  
671 Driving Cocaine Seeking. *The Journal of neuroscience : the official journal of the Society for*  
672 *Neuroscience* **39**, 2041-2051, doi:10.1523/JNEUROSCI.2822-18.2018 (2019).
- 673 39 Brog, J. S., Salyapongse, A., Deutch, A. Y. & Zahm, D. S. The patterns of afferent innervation of  
674 the core and shell in the "accumbens" part of the rat ventral striatum: immunohistochemical  
675 detection of retrogradely transported fluoro-gold. *J Comp Neurol* **338**, 255-278,  
676 doi:10.1002/cne.903380209 (1993).
- 677 40 Conte, W. L., Kamishina, H. & Reep, R. L. The efficacy of the fluorescent conjugates of cholera  
678 toxin subunit B for multiple retrograde tract tracing in the central nervous system. *Brain Struct*  
679 *Funct* **213**, 367-373, doi:10.1007/s00429-009-0212-x (2009).

- 680 41 Berthoud, H. R. & Munzberg, H. The lateral hypothalamus as integrator of metabolic and  
681 environmental needs: from electrical self-stimulation to opto-genetics. *Physiol Behav* **104**, 29-39,  
682 doi:10.1016/j.physbeh.2011.04.051 (2011).
- 683 42 Sweet, D. C., Levine, A. S., Billington, C. J. & Kotz, C. M. Feeding response to central orexins.  
684 *Brain research* **821**, 535-538, doi:10.1016/s0006-8993(99)01136-1 (1999).
- 685 43 Qu, D. *et al.* A role for melanin-concentrating hormone in the central regulation of feeding  
686 behaviour. *Nature* **380**, 243-247, doi:10.1038/380243a0 (1996).
- 687 44 Kopp, W. *et al.* Low leptin levels predict amenorrhea in underweight and eating disordered  
688 females. *Mol Psychiatry* **2**, 335-340, doi:10.1038/sj.mp.4000287 (1997).
- 689 45 Li, Z., Kelly, L., Heiman, M., Greengard, P. & Friedman, J. M. Hypothalamic Amylin Acts in  
690 Concert with Leptin to Regulate Food Intake. *Cell Metab* **23**, 945,  
691 doi:10.1016/j.cmet.2016.04.014 (2016).
- 692 46 Jennings, J. H., Rizzi, G., Stamatakis, A. M., Ung, R. L. & Stuber, G. D. The inhibitory circuit  
693 architecture of the lateral hypothalamus orchestrates feeding. *Science* **341**, 1517-1521,  
694 doi:10.1126/science.1241812 (2013).
- 695 47 Wickersham, I. R., Finke, S., Conzelmann, K. K. & Callaway, E. M. Retrograde neuronal tracing  
696 with a deletion-mutant rabies virus. *Nat Methods* **4**, 47-49, doi:10.1038/nmeth999 (2007).
- 697 48 Friedman, J. M. The function of leptin in nutrition, weight, and physiology. *Nutr Rev* **60**, S1-14;  
698 discussion S68-84, 85-17, doi:10.1301/002966402320634878 (2002).
- 699 49 Morton, G. J., Cummings, D. E., Baskin, D. G., Barsh, G. S. & Schwartz, M. W. Central nervous  
700 system control of food intake and body weight. *Nature* **443**, 289-295, doi:10.1038/nature05026  
701 (2006).
- 702 50 Myers, M. G., Jr., Munzberg, H., Leininger, G. M. & Leshan, R. L. The geometry of leptin  
703 action in the brain: more complicated than a simple ARC. *Cell Metab* **9**, 117-123,  
704 doi:10.1016/j.cmet.2008.12.001 (2009).
- 705 51 Cohen, P. *et al.* Selective deletion of leptin receptor in neurons leads to obesity. *J Clin Invest* **108**,  
706 1113-1121, doi:10.1172/JCI13914 (2001).
- 707 52 de Luca, C. *et al.* Complete rescue of obesity, diabetes, and infertility in db/db mice by neuron-  
708 specific LEPR-B transgenes. *J Clin Invest* **115**, 3484-3493, doi:10.1172/JCI24059 (2005).
- 709 53 Kim, K. S. *et al.* Enhanced hypothalamic leptin signaling in mice lacking dopamine D2 receptors.  
710 *The Journal of biological chemistry* **285**, 8905-8917, doi:10.1074/jbc.M109.079590 (2010).
- 711 54 Floresco, S. B. The nucleus accumbens: an interface between cognition, emotion, and action.  
712 *Annu Rev Psychol* **66**, 25-52, doi:10.1146/annurev-psych-010213-115159 (2015).
- 713 55 Johnson, P. M. & Kenny, P. J. Dopamine D2 receptors in addiction-like reward dysfunction and  
714 compulsive eating in obese rats. *Nature neuroscience* **13**, 635-641, doi:10.1038/nn.2519 (2010).
- 715 56 Wang, G. J. *et al.* Brain dopamine and obesity. *Lancet* **357**, 354-357, doi:10.1016/s0140-  
716 6736(00)03643-6 (2001).
- 717 57 Gerfen, C. R. Segregation of D1 and D2 dopamine receptors in the striatal direct and indirect  
718 pathways: An historical perspective. *Front Synaptic Neurosci* **14**, 1002960,  
719 doi:10.3389/fnsyn.2022.1002960 (2022).
- 720 58 Zhao, Z.-d. *et al.* A molecularly defined D1 medium spiny neuron subtype negatively regulates  
721 cocaine addiction. *Science Advances* **8**, eabn3552 (2022).
- 722 59 Zhou, K. *et al.* Reward and aversion processing by input-defined parallel nucleus accumbens  
723 circuits in mice. *Nat Commun* **13**, 6244, doi:10.1038/s41467-022-33843-3 (2022).
- 724 60 Mickelsen, L. E. *et al.* Single-cell transcriptomic analysis of the lateral hypothalamic area reveals  
725 molecularly distinct populations of inhibitory and excitatory neurons. *Nature neuroscience* **22**,  
726 642-656, doi:10.1038/s41593-019-0349-8 (2019).
- 727 61 Thoeni, S., Loureiro, M., O'Connor, E. C. & Lüscher, C. Depression of Accumbal to Lateral  
728 Hypothalamic Synapses Gates Overeating. *Neuron*, doi:10.1016/j.neuron.2020.03.029 (2020).
- 729 62 Elmquist, J. K., Bjorbaek, C., Ahima, R. S., Flier, J. S. & Saper, C. B. Distributions of leptin  
730 receptor mRNA isoforms in the rat brain. *J Comp Neurol* **395**, 535-547 (1998).

- 731 63 de Vrind, V. A. J., Rozeboom, A., Wolterink-Donselaar, I. G., Luijendijk-Berg, M. C. M. & Adan,  
732 R. A. H. Effects of GABA and Leptin Receptor-Expressing Neurons in the Lateral Hypothalamus  
733 on Feeding, Locomotion, and Thermogenesis. *Obesity (Silver Spring)* **27**, 1123-1132,  
734 doi:10.1002/oby.22495 (2019).
- 735 64 Jo, Y.-H., Chen, Y.-J. J., Chua, S. C., Talmage, D. A. & Role, L. W. Integration of  
736 endocannabinoid and leptin signaling in an appetite-related neural circuit. *Neuron* **48**, 1055-1066  
737 (2005).
- 738 65 Kirouac, G. J. Placing the paraventricular nucleus of the thalamus within the brain circuits that  
739 control behavior. *Neurosci Biobehav Rev* **56**, 315-329, doi:10.1016/j.neubiorev.2015.08.005  
740 (2015).
- 741 66 Millan, E. Z., Ong, Z. & McNally, G. P. in *Progress in Brain Research* Vol. 235 (eds Tanya  
742 Calvey & William M. U. Daniels) 113-137 (Elsevier, 2017).
- 743 67 Otis, J. M. *et al.* Paraventricular Thalamus Projection Neurons Integrate Cortical and  
744 Hypothalamic Signals for Cue-Reward Processing. *Neuron* **103**, 423-431 e424,  
745 doi:10.1016/j.neuron.2019.05.018 (2019).
- 746 68 Labouebe, G., Boutrel, B., Tarussio, D. & Thorens, B. Glucose-responsive neurons of the  
747 paraventricular thalamus control sucrose-seeking behavior. *Nature neuroscience* **19**, 999-1002,  
748 doi:10.1038/nn.4331 (2016).
- 749 69 Kessler, S. *et al.* Glucokinase neurons of the paraventricular nucleus of the thalamus sense  
750 glucose and decrease food consumption. *iScience* **24**, 103122, doi:10.1016/j.isci.2021.103122  
751 (2021).
- 752 70 Krause, M., German, P. W., Taha, S. A. & Fields, H. L. A pause in nucleus accumbens neuron  
753 firing is required to initiate and maintain feeding. *The Journal of neuroscience : the official*  
754 *journal of the Society for Neuroscience* **30**, 4746-4756, doi:10.1523/JNEUROSCI.0197-10.2010  
755 (2010).
- 756 71 Kelley, A. E. Ventral striatal control of appetitive motivation: role in ingestive behavior and  
757 reward-related learning. *Neurosci Biobehav Rev* **27**, 765-776,  
758 doi:10.1016/j.neubiorev.2003.11.015 (2004).
- 759 72 Richardson, N. R. & Roberts, D. C. Progressive ratio schedules in drug self-administration  
760 studies in rats: a method to evaluate reinforcing efficacy. *Journal of neuroscience methods* **66**, 1-  
761 11, doi:10.1016/0165-0270(95)00153-0 (1996).

762

## 763 764 **Acknowledgements**

765 The authors thank Dr. Chao Zhang for his help in generating Fig. 1a; Dr. Jeffrey M. Friedman  
766 for discussion on some experiments; Dr. Aritra Bhattachajee for critical reading of the  
767 manuscript. We thank the Mouse Behavior Core of Harvard Medical School and its director Dr.  
768 Barbara Caldarone for her help. This project was partly supported by 1R01DA042283,  
769 1R01DA050589, and HHMI. Y.Z. is an investigator of the Howard Hughes Medical Institute.  
770 This article is subject to HHMI's Open Access to Publications policy. HHMI lab heads have  
771 previously granted a nonexclusive CC BY 4.0 license to the public and a sublicensable license to  
772 HHMI in their research articles. Pursuant to those licenses, the author-accepted manuscript of



773 this article can be made freely available under a CC BY 4.0 license immediately upon  
774 publication.

775

## 776 **Author information**

---

777 Authors and Affiliations

778 **Howard Hughes Medical Institute, Boston Children's Hospital, Boston, MA, USA**

779 Yiqiong Liu, Zheng-dong Zhao, Guoguang Xie, Renchao Chen and Yi Zhang

780 **Program in Cellular and Molecular Medicine, Boston Children's Hospital, Boston, MA,**  
781 **USA**

782 Yiqiong Liu, Zheng-dong Zhao, Guoguang Xie, Renchao Chen and Yi Zhang

783 **Division of Hematology/Oncology, Department of Pediatrics, Boston Children's Hospital,**  
784 **Boston, MA, USA**

785 Yiqiong Liu, Zheng-dong Zhao, Guoguang Xie, Renchao Chen and Yi Zhang

786 **Department of Genetics, Harvard Medical School, Boston, MA, USA**

787 Yi Zhang

788 **Harvard Stem Cell Institute, WAB-149G, 200 Longwood Avenue, Boston, MA, USA**

789 Yi Zhang

790

## 791 **Contributions**

792 Y.Z. conceived the project; Y.L., and Y.Z. designed the experiments; Y.L. performed most of the  
793 experiments. Z.-D.Z. helped with the fiber photometry. G.X. helped with the catheter  
794 administration. R.C. initiated the Serpinb2-Cre mouse generation. Y.L., Z.-D.Z., R.C. and Y.Z.  
795 interpreted the data; Y.L. and Y.Z. wrote the manuscript with input from Z.-D.Z and R. C.

796

797

## 798 **Ethics declarations**

### 799 **Competing interests**

---

800 The authors declare no competing interests.

801

802 **Figure Legends**

803

804 **Fig. 1: NAcSh *Serpinb2*<sup>+</sup> neurons and NAc *Drd1*<sup>+</sup>-MSNs are activated in refeeding process**

805 **a**, Inferred spatial expression patterns from MERFISH database of *Tac2*, *Serpinb2* and *Ubp1*  
806 whose expression is highly enriched in medial dorsal NAc shell. Expression level is color-  
807 coded. Dotted line circle anterior commissure olfactory limb (aco) and NAc core. The dorsal-  
808 ventral (DV) and medial-lateral (ML) axes are indicated.

809 **b**, Left, tSNE plot showing the 8 NAc D1-MSN subtypes. Middle and right panels indicate the  
810 expression of *Tac2* and *Serpinb2* in the NAc D1-MSNs, respectively. Expression level is  
811 color-coded.

812 **c**, RNA *in situ* hybridization showing *Tac2* and *Serpinb2* expression in the medial part of the  
813 NAc shell. Scale bar: 500  $\mu$ m (left), 20  $\mu$ m (right).

814 **d**, Schematic representation of the experimental design for the ad libitum, fast and refed groups.

815 **e**, Coexpression of *Serpinb2* mRNA with *cFos* mRNA in NAc of ad libitum, fasted and refed  
816 states. Representative images showing the colocalization of *cFos* (green), *Serpinb2* (red) and  
817 *Tac2* (magenta) expressing neurons. Scale bar: 50  $\mu$ m.

818 **f**, The average number of *cFos*<sup>+</sup> neurons in the dorsal medial NAcSh at ad libitum, fasted and  
819 refed states. (n = 5 sections from three mice of each group, one-way ANOVA, with Tukey's  
820 multiple comparisons).

821 **g**, The percentages of activated *Serpinb2*-expressing neurons in the total *Serpinb2* neurons under  
822 different feeding states (n = 5 sections from three mice of each group, one-way ANOVA,  
823 with Tukey's multiple comparisons).

824 **h**, The percentages of activated *Tac2*-expressing neurons in the total *Tac2* neurons under  
825 different feeding states (n = 5 sections from three mice of each group, one-way ANOVA,  
826 with Tukey's multiple comparisons). All error bars represent mean  $\pm$  SEM. ns, not significant,  
827 \*P < 0.05.

828

829 **Fig. 2: The activity of *Serpinb2*<sup>+</sup> neurons respond to feeding states**

830 **a**, Left, illustration of light pathways of fiber photometry. Right, schematic illustration of the  
831 GCaMP7s injection and optic cannula implantation.

832 **b, c**, Validation of GCaMP7s expression and implantation of optic cannula in *Serpib2*-Cre mice  
833 (b) or *Drd1*-Cre mice (c) (left). Representative trace of real-time monitoring of *Serpib2*<sup>+</sup>  
834 neurons (b) or *Drd1*<sup>+</sup> neurons (c) (right) during feeding process. Scale bar: 200  $\mu$ m.  
835 **d**, Ca<sup>2+</sup> signals at different phases of feeding process of fasted mice (top). Average Ca<sup>2+</sup> signal at  
836 different feeding phases of the *Serpib2*-Cre mice. Elevated Ca<sup>2+</sup> signals were observed after  
837 entering food zone in approaching and eating phases. Declined Ca<sup>2+</sup> signals were observed  
838 post eating. Quantification of AUC in the four phases is shown in bar graph (right, n=7).  
839 **e**, The same as in panel D except *Drd1*-Cre mice were used. \*\*\*P  $\leq$  0.001, \*\*P  $\leq$  0.01, \*P  $\leq$  0.05;  
840 ns, P > 0.05, one-way ANOVA test. Data are represented as mean  $\pm$  SEM.

841  
842 **Fig. 3: *Serpib2*<sup>+</sup> neurons bidirectionally regulate food seek and intake in hungry state**

843 **a**, Experimental scheme of the food consumption and food preference assays.  
844 **b**, Total food consumption during the 3-hour test. Chemogenetic activation (hM3Dq) or  
845 chemogenetic inhibition (hM4Di) of *Serpib2*<sup>+</sup> neurons at ad libitum (left) or fasting state  
846 (right). \*\*, p<0.01; ns, p>0.05, unpaired t-test.  
847 **c**, The same as in panel B except the *Tac2*-Cre (left) or *Drd1*-Cre (right) mice were used. ns,  
848 p>0.05, unpaired t-test.  
849 **d**, Color map encoding spatial location of a fasted mouse using the free access feeding paradigm.  
850 **e**, Percentage of time that mice spent in food zone. Chemogenetic activation (hM3Dq) or  
851 chemogenetic inhibition (hM4Di) of *Serpib2*<sup>+</sup> neurons (left), *Tac2*<sup>+</sup> neurons (middle), and  
852 *Drd1*<sup>+</sup> neurons (right). \*, p<0.05; ns, p>0.05, unpaired t-test.  
853 **f**, Experimental timeline of the food operant chamber assay.  
854 **g**, Diagrammatic illustration of the food operant chamber paradigm. Mice were trained to press  
855 the lever to get food; pressing the active lever is followed by the delivery of food pellet,  
856 while pressing the inactive lever yields no outcome. The behavioral training includes  
857 habituation phase and fixed ratio (FR) training phase. Mice received CNO injection (2 mg/kg  
858 for the hM3Dq group and 5 mg/kg for the hM4Di group) 15 mins before they were placed  
859 into the operant chamber to start the FR and progressive ratio (PR) tests.  
860 **h**, Results of FR=5 test. The total number of active lever pressing (left) and total number of  
861 reward (right) after chemogenetic manipulations. \*\*, p<0.01; \*, p<0.05; ns, p>0.05; one-way  
862 ANOVA test.

863 **i**, Results of PR=5 test. The total number of active lever pressing (left) and total number of  
864 reward (right) after chemogenetic manipulations. \*,  $p < 0.05$ ; ns,  $p > 0.05$ ; one-way ANOVA  
865 test.

866 Data are represented as mean  $\pm$  SEM.

867

868 **Fig. 4: *Serpib2*<sup>+</sup> neurons mediate food intake via LH projection**

869 **a**, Diagram of anterograde tracing of the NAc *Serpib2*<sup>+</sup> neurons with ChR2-EYFP (left), the  
870 expression of DIO-ChR2-EYFP in the NAcSh (2<sup>nd</sup> panel), and *Serpib2*<sup>+</sup> neuron projection  
871 to LH (the right 3 panels). Scale bar: 100  $\mu$ m.

872 **b**, Diagram (left) and image (right) of retrograde tracing of LH neurons with CTB 647, with the  
873 *Serpib2*<sup>+</sup> neurons labeled by DIO-mCherry. Scale bar: 50  $\mu$ m.

874 **c**, Percentage of *Serpib2*<sup>+</sup> LH projecting neurons over the total mCherry labeled *Serpib2*<sup>+</sup>  
875 neurons.

876 **d**, Diagram illustrate the indicated AAV injection into NAc and optic cannulas implantation in  
877 LH area (left), and histology validating virus expression and cannula implantation site (right).  
878 Scale bar: 200  $\mu$ m.

879 **e**, Optogenetic activation (left) or inhibition (right) of *Serpib2*<sup>+</sup> NAc→LH neurons respectively  
880 increased or decreased food intake.

881 Data in (e) is presented as mean  $\pm$  SEM. TH, thalamus, CP, caudoputamen, AHNc: anterior  
882 hypothalamic nucleus, central part, HPF, hippocampal formation, VL, lateral ventricle. \*\*\* $P$   
883  $\leq 0.001$ ; \* $P \leq 0.05$ ; ns,  $P > 0.05$ , unpaired t-test.

884

885 **Fig. 5: *Serpib2*<sup>+</sup> neurons project to LH LepR<sup>+</sup> GABA<sup>+</sup> neurons and receive input related**  
886 **to energy homeostasis**

887 **a**, Diagram indicating the MCH<sup>+</sup>, Orexin-A<sup>+</sup>, GABA<sup>+</sup> and LepR<sup>+</sup> neurons in LH.

888 **b**, Images (left two panels) showing colocalization of *Serpib2*<sup>+</sup> neuron terminals (green) with  
889 MCH<sup>+</sup>, Orexin-A<sup>+</sup> neurons in LH, and their quantifications (right panel). Scale bar, 50  $\mu$ m.  
890 Percentage =  $eYFP^+MCH^+/eYFP^+DAPI^+$  or  $eYFP^+Orexin-A^+/eYFP^+DAPI^+$

891 **c**, Images showing the colocalization of *Serpib2*<sup>+</sup> neuron terminals (green) with GABA<sup>+</sup> (red)  
892 or LepR<sup>+</sup> neurons (red) as indicated, as well as their quantifications (right panel). Scale bar,  
893 50  $\mu$ m. Percentage =  $eYFP^+GABA^+/eYFP^+DAPI^+$  or  $eYFP^+LepR^+/eYFP^+DAPI^+$

894  
895 **d**, Quantification of cFos<sup>+</sup> cells of different brain regions in ad libitum and refeed status. (n = 3  
896 sections from three mice of each group, unpaired t-test)  
897 **e**, Schematic presentation of modified rabies tracing (left) and representative image confirming  
898 the expression of the indicated proteins at the injection site (right); scale bar, 100 μm  
899 (left); 20μm (right).  
900 **f**, Representative images showing the brain areas with positive signals indicating these regions  
901 have neurons projecting to *Serpinb2*<sup>+</sup> neurons. Scale bar: 100 μm, arrow heads indicate  
902 neurons.  
903 **g**, Diagram illustrating brain regions upstream and downstream of *Serpinb2*<sup>+</sup> neurons.  
904 ACAAd: Anterior cingulate area, dorsal part; fa, corpus callosum, anterior forceps; LPO: lateral  
905 preoptic area; SI: substantia innominata; PVT: paraventricular nucleus of the thalamus; VMH:  
906 ventromedial hypothalamic nucleus; LH: lateral hypothalamus; V3: third ventricle.  
907  
908 **Fig. 6: Modulating *Serpinb2*<sup>+</sup> neuron activity can overcome leptin effect and alter**  
909 **bodyweight**  
910 **a**, Diagram showing bilateral cannula implantation in LH for leptin delivery (left). CNO delivery  
911 was achieved via i.p. injection. Results of total food consumption in 3 hours by fasted mice  
912 with different doses of leptin administration. Scale bar: 500 μm.  
913 **b**, Same as panel A except food consumption is quantified under different conditions with or  
914 without *Serpinb2*<sup>+</sup> neuron activation in the presence or absence of 1 μg of leptin delivery.  
915 \*\*\*P ≤ 0.001, \*\*P ≤ 0.01, \*P ≤ 0.05; ns, P > 0.05, unpaired t-test.  
916 **c**, FISH and quantification verify *Serpinb2*<sup>+</sup> neuron ablation after AAV-DIO-taCasp3 injection.  
917 Scale bar: 100 μm. \*\*\*P ≤ 0.001, unpaired t-test.  
918 **d**, *Serpinb2*<sup>+</sup> neuron ablation decreased 3 hours total food consumption by mice. \*\*\*P ≤ 0.001,  
919 unpaired t-test.  
920 **e**, *Serpinb2*<sup>+</sup> neuron ablation has a long-time effect on bodyweight loss. \*\*\*P ≤ 0.001, \*\*P ≤  
921 0.01, \*P ≤ 0.05; ns, P > 0.05, unpaired t-test.  
922 Data are presented as means ± SEM.

923 **Extended Data Figure Legends**

924

925 **Extended Data Fig. 1: Generation and validation of *Serpib2*-Cre line**

926 **a**, Diagrams showing the targeting strategy.

927 **b**, Genotyping by PCR. Homozygotes: 413 bp. Heterozygotes: 413 bp/772 bp.

928 **c**, Left, in situ hybridization (ISH) data of *Serpib2* from Allen Brain Atlas. Scale bar: 1000  $\mu\text{m}$ .

929 Middle, colocalization of *Serpib2* RNA (red), AAV-DIO-ChR2-eYFP (green) and DAPI

930 (blue). Scale bar: 50  $\mu\text{m}$ . Right, quantification of *Serpib2*<sup>+</sup> and eYFP<sup>+</sup> neurons among all

931 *Serpib2*<sup>+</sup> neurons.

932

933 **Extended Data Fig. 2: *Serpib2*<sup>+</sup> neuron activity during different phases of feeding in ad**

934 **libitum mice**

935 **a**, Ca<sup>2+</sup> signals at different phases of feeding process of ad libitum mice (top). Average Ca<sup>2+</sup>

936 signal at different feeding phases of the *Serpib2*-Cre mice. Elevated Ca<sup>2+</sup> signals were

937 observed after entering food zone in the approaching and eating phases. Declined Ca<sup>2+</sup>

938 signals were observed post eating. Quantification of AUC in the four phases is shown in bar

939 graph (right, n=7 mice).

940 **b**, The same as in panel D except *Drd1*-Cre mice were used.

941 \*\*P  $\leq$  0.01, \*P  $\leq$  0.05; ns, P > 0.05, one-way ANOVA test. Data are represented as mean  $\pm$  SEM.

942

943 **Extended Data Fig. 3: Validation of chemogenetic manipulation**

944 **a**, Experimental scheme of chemogenetic manipulation.

945 **b**, Validation of virus expression in *Serpib2*-Cre, *Tac2*-Cre and *Drd1*-Cre mice. Scale bar: 500

946  $\mu\text{m}$ .

947 **c**, *cFos* induction after intraperitoneal injection of ligand CNO in mCherry-expressing, hM3Dq-

948 mCherry-expressing and hM4Di-mCherry-expressing mice. The ratio of cFos<sup>+</sup>/mCherry<sup>+</sup>

949 cells in all mCherry<sup>+</sup> cells was calculated and shown on the right panel. Scale bar: 100  $\mu\text{m}$ . \*,

950 p < 0.05; \*\*, p < 0.01, one-way ANOVA test. Data are represented as mean  $\pm$  SEM.

951

952 **Extended Data Fig. 4: *Serpib2*<sup>+</sup> neuronal activity does not affect anxiety or drug seeking**

953 **behavior**

954 **a, b**, Open field test for the effect of *Sepinb2*<sup>+</sup> neuronal activation (hM3Dq) (a) or inhibition  
955 (hM4Di) (b) on the total distance traveled in the 1-hour post-treatment period after  
956 chemogenetic manipulation of *Sepinb2*<sup>+</sup> neurons (left) or the distance traveled in 5-min time  
957 bin (right).

958 ns,  $p > 0.05$ , left, unpaired t-test; right, two-way ANOVA.

959 **c**, Left, illustration of the two-chamber cocaine-CPP paradigm. Right, cocaine-CPP with  
960 chemogenetic activation (hM3Dq) or inhibition (hM4Di) of *Sepinb2*<sup>+</sup> neurons. CPP scores  
961 were calculated by subtracting the time spent in the preconditioning phase from the time  
962 spent in the postconditioning phase. ns,  $p > 0.05$ , unpaired t-test.

963 **d, e**, Elevated plus maze test for the effect of *Sepinb2*<sup>+</sup> neuronal activation (hM3Dq) (d) or  
964 inhibition (hM4Di) (e) on the time spent (left) or distance traveled (right) in open arm and  
965 closed arm of the 5-min post-treatment period after chemogenetic manipulation of *Sepinb2*<sup>+</sup>  
966 neurons. ns,  $p > 0.05$ , unpaired t-test.

967 Data are represented as mean  $\pm$  SEM.

968

969 **Extended Data Fig. 5: cFos staining of different brain regions from mice under Ad libitum**  
970 **and refeed states**

971 Shown are cFos FISH in different brain regions listed below:

972 ACB: Nucleus accumbens; aco: anterior commissure, olfactory limb; OT:

973 Olfactory tubercle; V3: third ventricle; ARH: Arcuate hypothalamic nucleus; AHNp: Anterior

974 hypothalamic nucleus, posterior part; VMH: ventromedial hypothalamic nucleus; fx: columns of

975 the fornix; LH: lateral hypothalamus; PVT: paraventricular nucleus of the thalamus; sm: stria

976 medullaris; BLA: Basolateral amygdala; LA: Lateral amygdala; RE: Nucleus of reuniens; DMH:

977 Dorsomedial nucleus of the hypothalamus; ZI: Zona incerta. Scale bar: 100  $\mu$ m.

978

979 **Extended Data Fig. 6: Brain regions that do not innervate *Serpib2*<sup>+</sup> neurons**

980 Shown are immunostaining of the various brain regions listed below:

981 PL: Prelimbic area; IL: Infralimbic area; fa: corpus callosum, anterior forceps; ccg: genu of  
982 corpus

983 callosum; LSr: Lateral septal nucleus, rostral part; VL: lateral ventricle; ACB: Nucleus

984 accumbens; aco: anterior commissure, olfactory limb; OT: Olfactory tubercle; ADP:

985 Anterodorsal preoptic nucleus; BST: Bed nuclei of the stria terminalis; V3: third ventricle; ARH:  
986 Arcuate hypothalamic nucleus; AHNp: Anterior hypothalamic nucleus, posterior part; VMH:  
987 ventromedial hypothalamic nucleus; fx: columns of the fornix; LH: lateral hypothalamus; PVT:  
988 paraventricular nucleus of the thalamus; sm: stria medullaris; BLA: Basolateral amygdala; LA:  
989 Lateral amygdala; RE: Nucleus of reuniens; DMH: Dorsomedial nucleus of the hypothalamus;  
990 ZI: Zona incerta; DG: Dentate gyrus; CA1: field CA1; CA3: field CA3; PAG: Periaqueductal  
991 gray ; APN: Anterior pretectal nucleus; HPF: Hippocampal formation. Scale bar: 100  $\mu$ m



**Fig. 1: NAcSh *Serpinb2*<sup>+</sup> neurons and NAc *Drd1*<sup>+</sup>-MSNs are activated in refeeding process.**

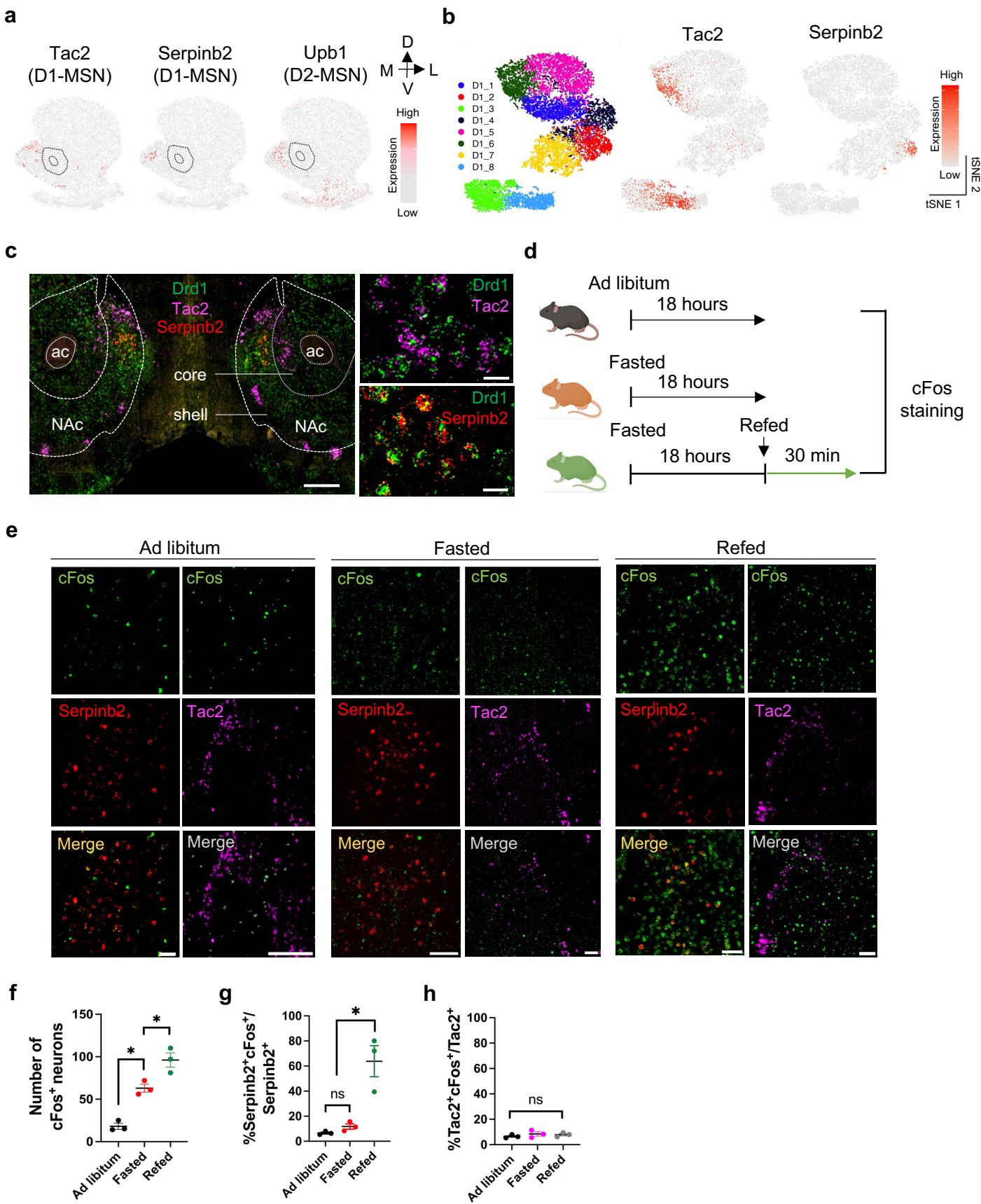


**Fig. 2: The activity of *Serpib2*<sup>+</sup> neurons respond to feeding states.**

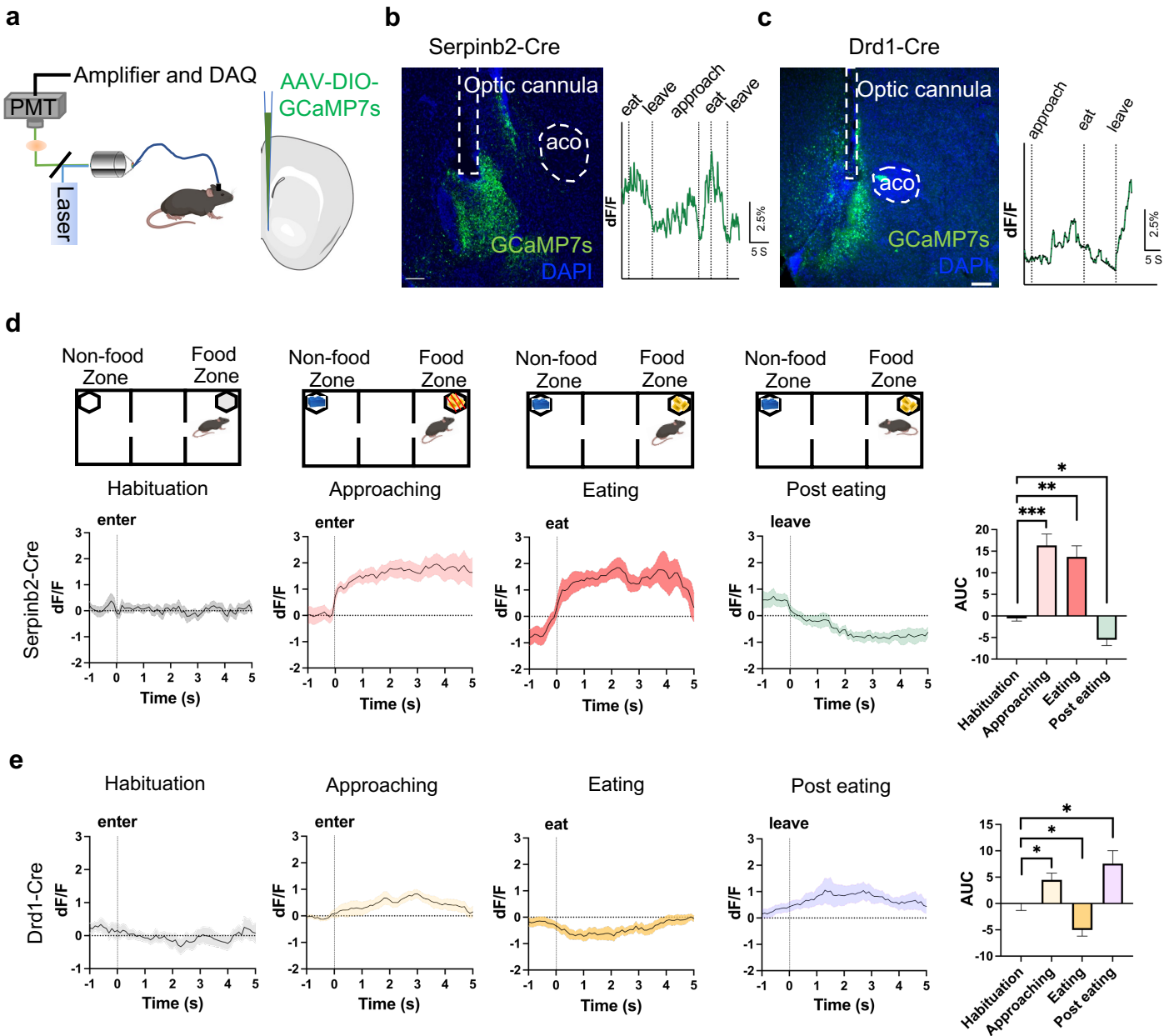


**Fig. 3: *Serpin2*<sup>+</sup> neurons bidirectionally regulate food seek and intake in hungry state.**

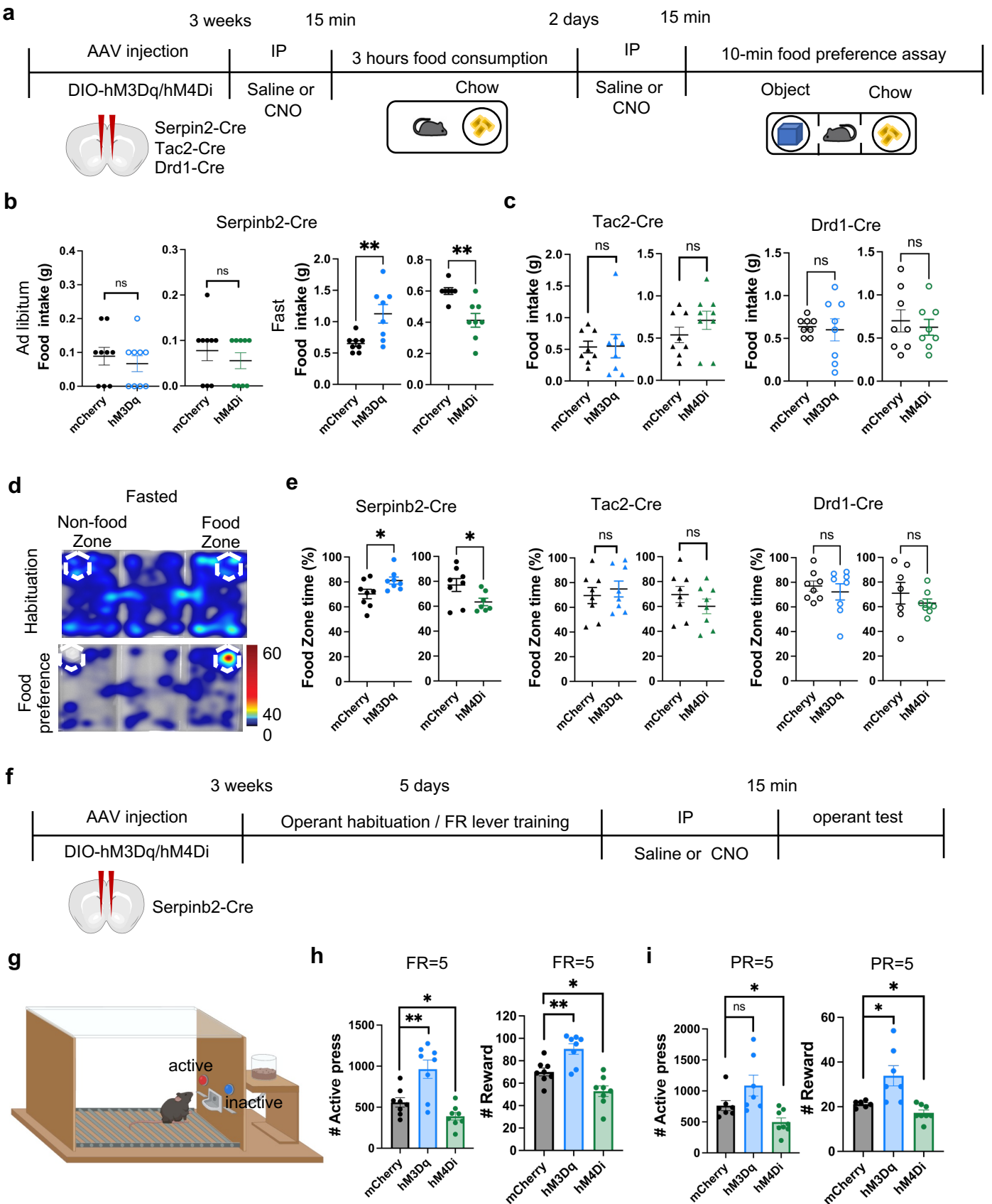


**Fig. 4: *Serpinb2*<sup>+</sup> neurons mediate food intake via LH projection.**

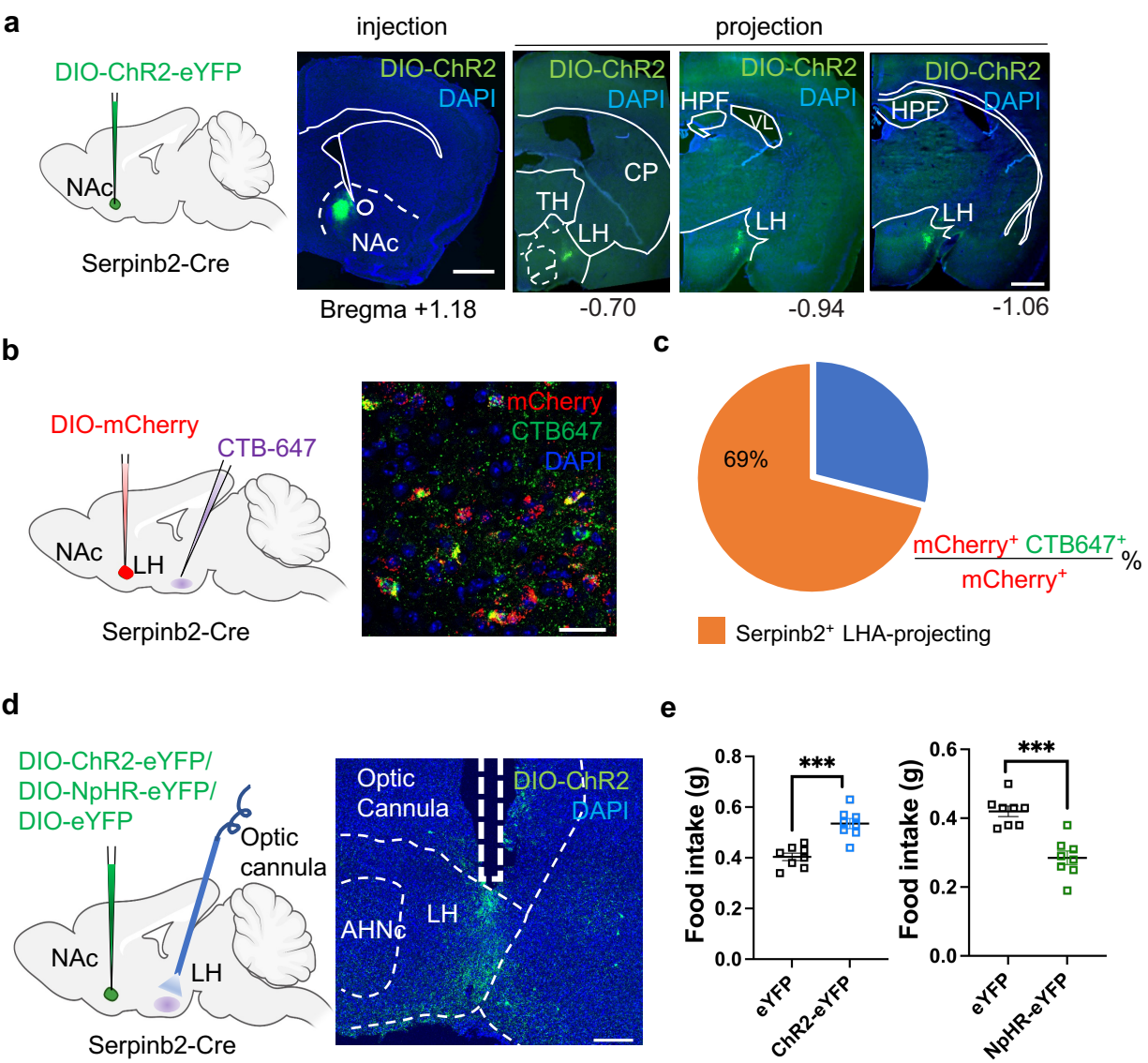


**Fig. 5: *Serpib2*<sup>+</sup> neurons project to LH LepR<sup>+</sup> GABA<sup>+</sup> neurons and receive input related to energy homeostasis.**

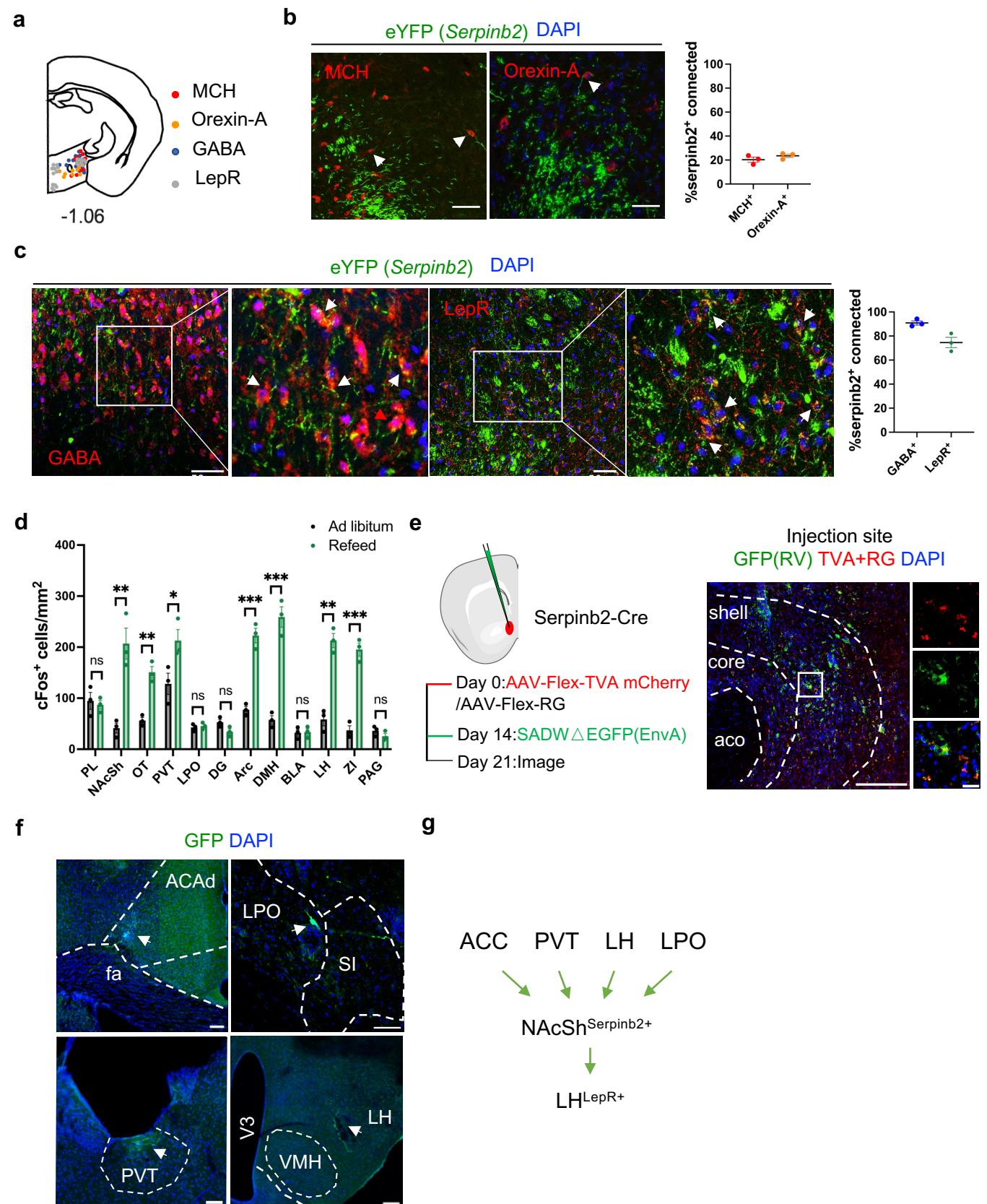
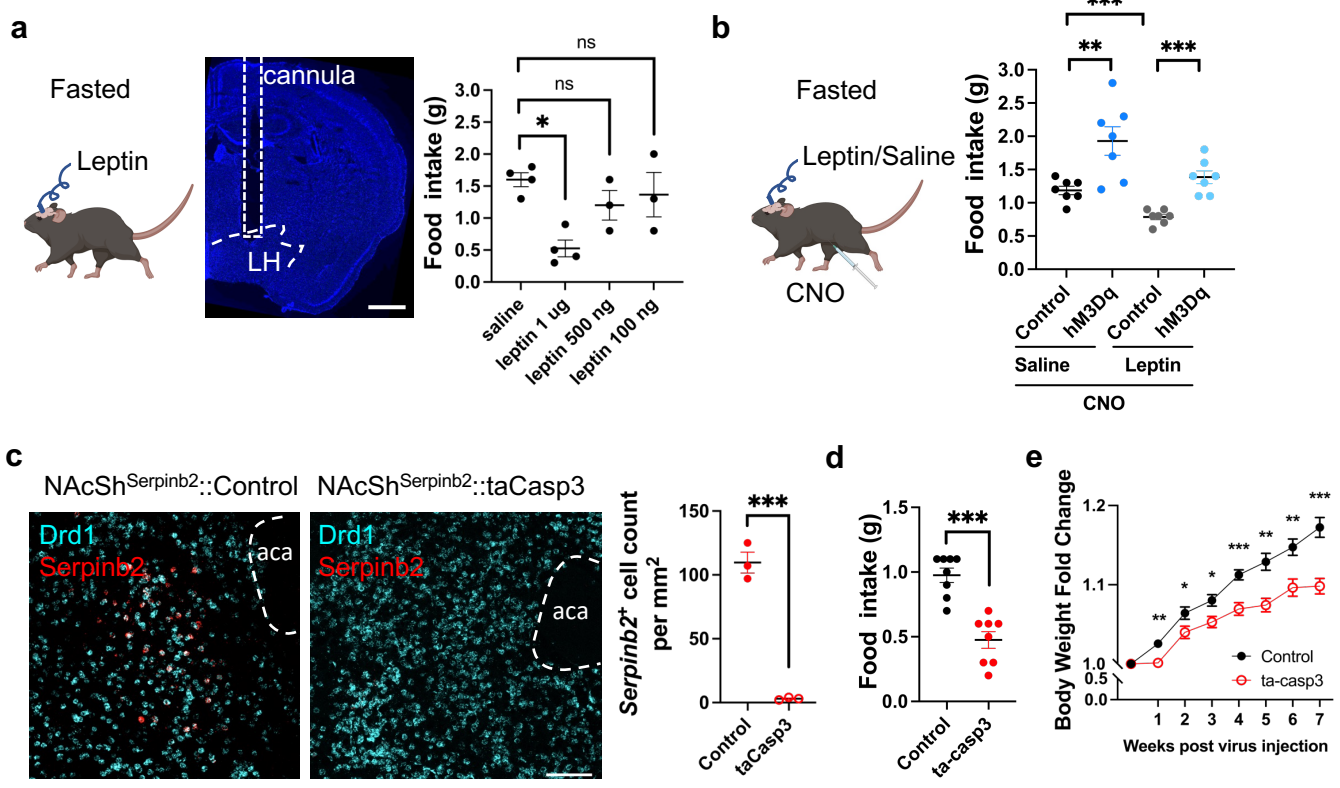
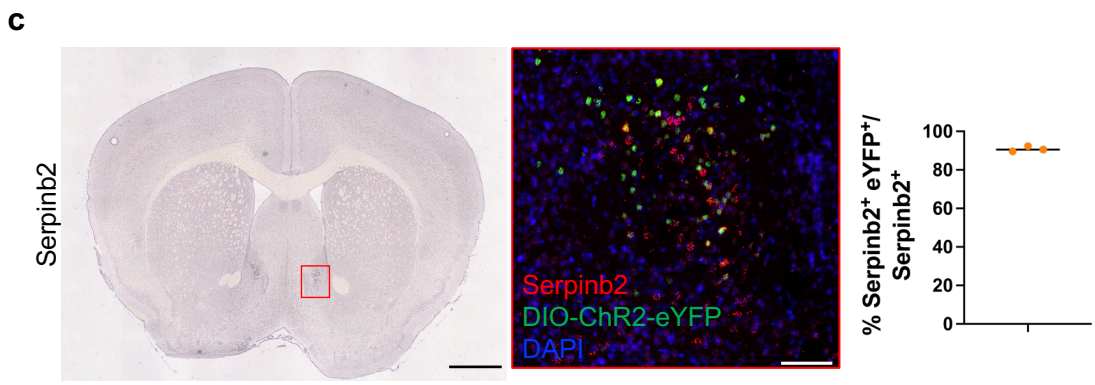
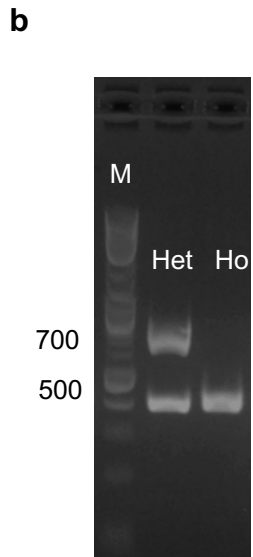
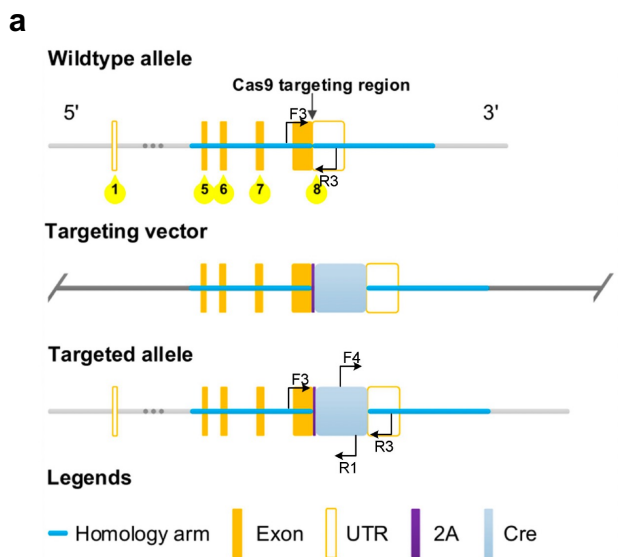


**Fig. 6: Modulating *Serpinb2*<sup>+</sup> neuron activity can overcome leptin effect and alter bodyweight.**



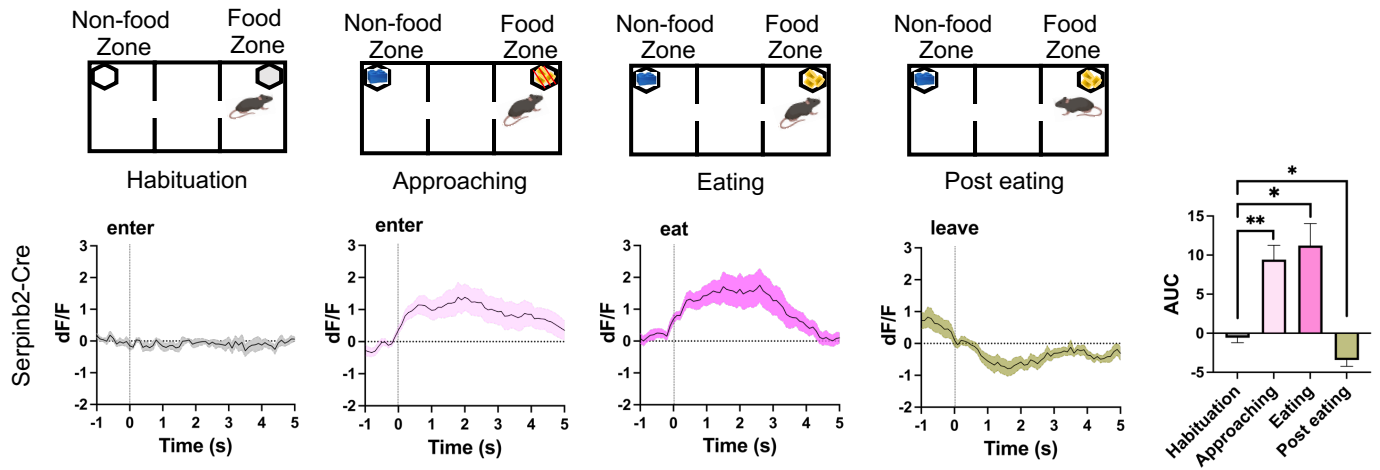
**Extended Data Fig. 1: Generation and validation of *Serpib2*-Cre line**



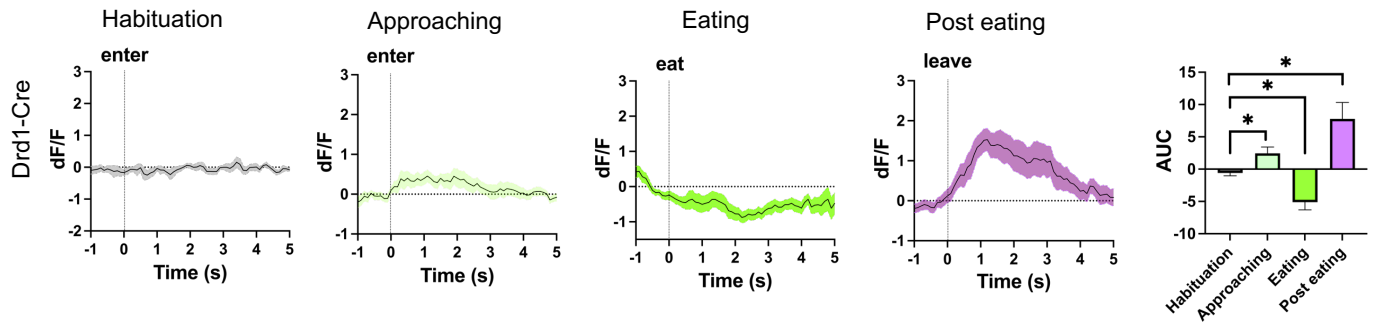
Extended Data Fig. 2: *Serpinb2*<sup>+</sup> neuron activity during different phases of feeding in ad libitum mice

**a**

Ad libitum

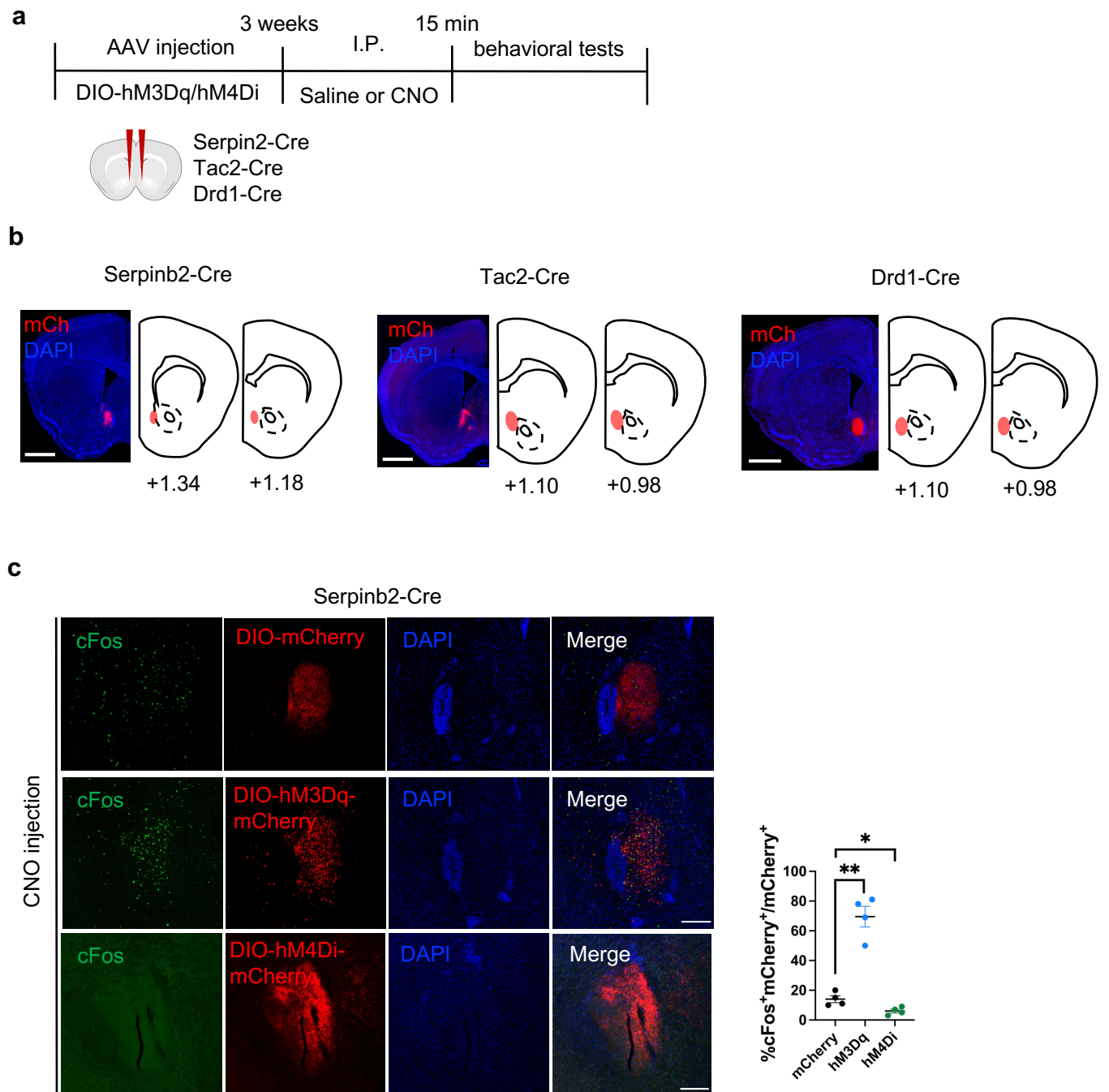


**b**

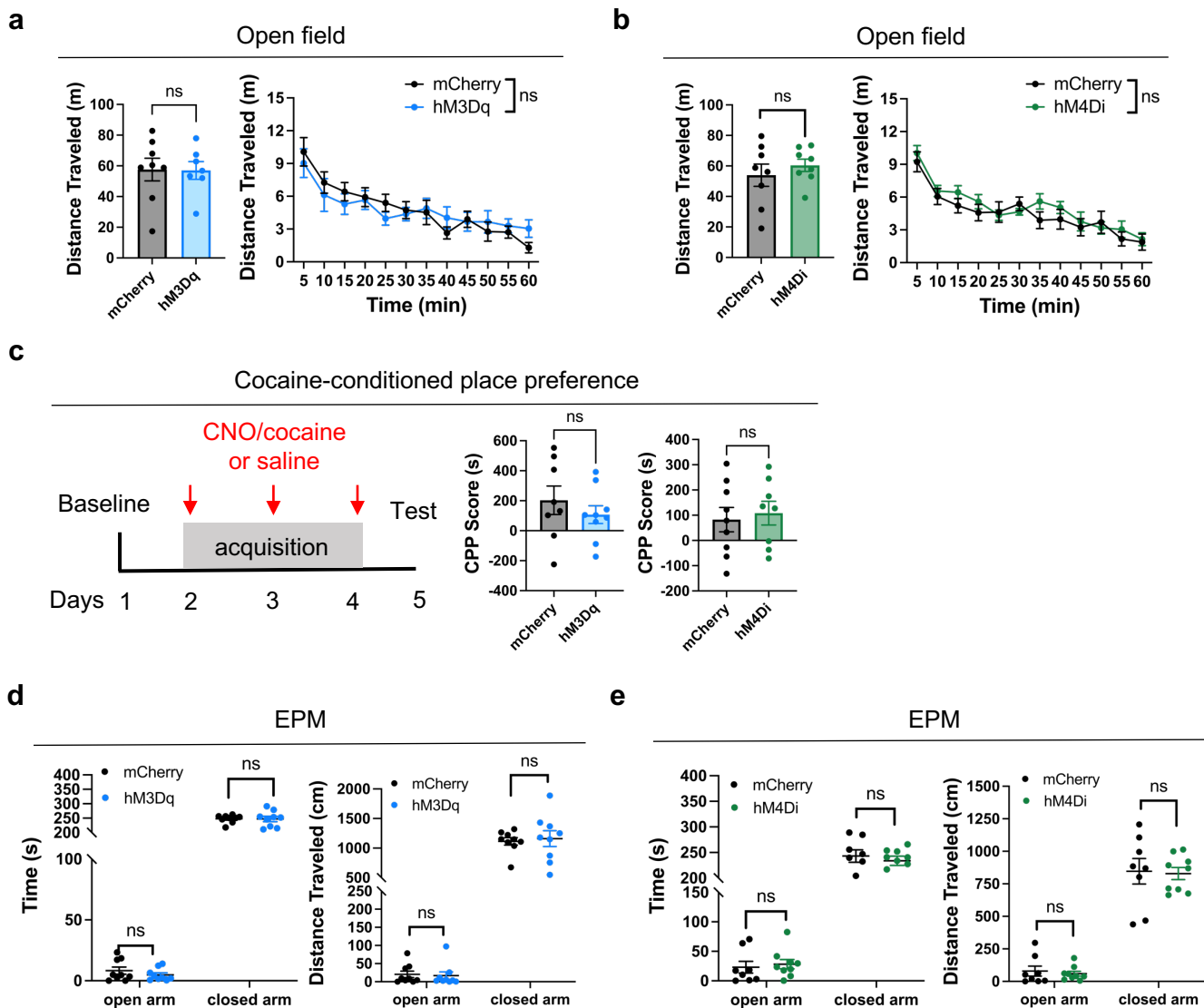




# Extended Data Fig. 3: Validation of chemogenetic manipulation

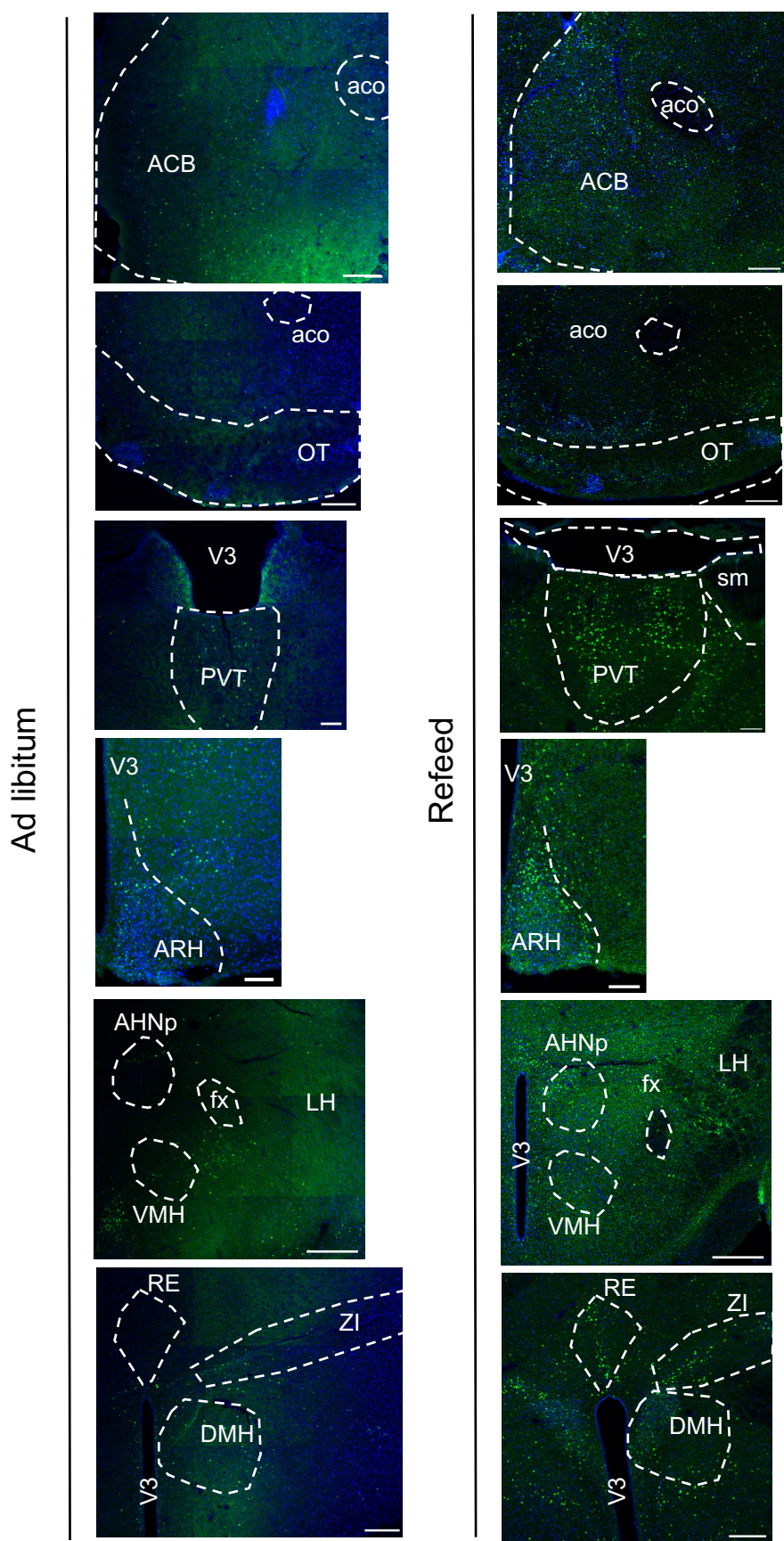


**Extended Data Fig. 4: *Serpib2*<sup>+</sup> neuronal activity does not affect anxiety or drug seeking behavior**



Extended Data Fig. 5: cFos staining of different brain regions from mice under Ad libitum and refeed states

cFos DAPI



Extended Data Fig. 6: Brain regions that do not innervate *Serpinb2*<sup>+</sup> neurons

cFos DAPI

